NANOSTURCTURED BIOMATERIALS FOR TISSUE REGENERATION AND REPAIR

by

PRIMANA PUNNAKITIKASHEM

Presented to the Faculty of the Graduate School of

The University of Texas at Arlington in Partial Fulfillment

of the Requirements

for the Degree of

DOCTOR OF PHILOSOPHY

THE UNIVERSITY OF TEXAS AT ARLINGTON

July 2016

Acknowledgements

My deeply and highly gratitude goes to my advisors, Dr. Yi Hong and Dr. Kytai Truong Nguyen, for their advice and help during my doctoral studies. They also introduced me to very interesting research topics and consistently helped me in my research. I appreciate their patience in addition to taking time to answer and guide me through many challenges in a professional way. I am highly grateful to my thesis committee members, Dr. Debabrata Saha, Dr. Alice Sun, and Dr. Liping Tang for spending time to help me during my thesis defense process. In addition, I would like to thank Dr. Connie Hsia and Dr. Baohong Yuan, for their encouragement and helpful advice in my research. I would also like to acknowledge the help from all my lab mates, and the other lab members in Drug Delivery Lab, Tissue Engineering and Biomaterials Lab, and Characterization Center for Materials & Biology. I highly appreciate to all my family members for their inspiration, and persistent support. I am indebted to the loving memory of my grandmother and my aunt for their love and support during my Ph.D. career. I also want to express my sincere appreciation to my family and relatives for their encouragement and supports.

Abstract

NANOSTURCTURED BIOMATERIALS FOR TISSUE REGENERATION AND REPAIR

Primana Punnakitikashem, PhD

The University of Texas at Arlington, 2016

Supervising Professors: Yi Hong and Kytai T. Nguyen

Nanostructured materials have been explored in biomedical field especially in tissue engineering over a past decade. This type of material can be processed into biomaterial scaffolds; revealed many advantages to be used in human living system such as restoring, healing, replacing and improving the function of interested tissues or organs. In this work, nanostructured materials were synthesized as a nanofibrous scaffold or nanoparticles, which were characterized and tested for their biofunctions in the regeneration of blood vessels, lung and skin tissues. Firstly, biodegradable polyurethane nanofibrous scaffolds with dipyramole were electrospun to create a vascular graft, and results demonstrated that this nanofibrous scaffold matched the native artery mechanical strength, reduced the platelet deposition, improved blood compatibility, supported endothelial cell formation and inhibited the proliferation of smooth muscle cells. Next, biodegradable polylactic-glycolic acid nanoparticles were fabricated and then coated with porcine lung extracellular matrix to maximize the nanoparticle deposition on the alveolar epithelial cells. These nanoparticles also show that they were cytocompatible with alveolar type I epithelial cells and facilitated the cellular retention/uptake. Preliminary studies of electrospun nanofibrous polyurethane scaffold incorporated with nanoparticles loaded with anti-microbial peptide and/or antibiotics for wound healing application

demonstrated these nanostructured materials could be used to prevent bacterial infection and suggest their potential in skin wound healing applications. Results from this research suggest that the biomaterials either in the nanofiber or nanoparticle structures could be used for regeneration of various tissue organs such as blood vessels and skins, and for protein (growth factors) or gene therapy (cDNA plasmids) delivery to facilitate lung regeneration. Hence, the nanostructured biomaterials would have high potential to be applied for tissue regeneration to manage diseased and damaged tissues/organs for human healthcare.

Table of Contents

List of Illustrations

List of Tables

Chapter 1

Introduction

1.1 Nanostructured biomaterials for biomedical applications

Nanotechnology in science and engineering has been developed over the past decade. Nanostructured materials apply to the structure of the small size of its material which in the range of 1-100 nanometer (nm). Not only are the sizes taking into account of nanostructured material, but also the functional, properties and side effect of the material are crucial and need to be investigated [1]. To create a nanostructured material for biomedical application, modified and combine the material with biological system such as protein, virus, and membrane cannot be neglected [2]. The material used for synthesizing the nanostructured material could be metal, ceramic, polymer, and organic materials. There are several types of nanostructured material used in biomedical applications; for instance, nanoparticles, nanofibers, nanoclusters, nanocrystals, nanotubes, nanowires, nanorods, nanofilms, and so on [3]. There are many methods to create or make new nanostructured materials, for example, electrospinning, phase separation, self-assembly processes, chemical vapor deposition, chemical etching, nano-imprinting, and photolithography [3]. To achieve the goal prior to biomedical applications, modification of nanostructured materials are also necessary [4].

The growth of the nanotechnology in biomedical applications is highly shown in various fields, mostly in tissue engineering which is presented as biomaterials, carriers for drug delivery system, and biosensors [4]. The biomaterial is a natural or synthetic material, which can be used in human living tissues. It has been investigated and applied to human living tissues for the purpose of restoring, healing, replacing and improving the function of interested tissues and/or organs. Current biomaterials can be categorized by types of biomaterial which are devices and implants. The implants biomaterial (sutures,

ligaments, vascular grafts, heart valves, etc.) and device material (pacemakers, biosensors, and artificial hearts) are two majors biomaterial in biomedical applications for patients [5]. To implement biomaterial on specific tissues or organs, the biocompatibility of the biomaterial needs to be concerned. Hard tissue (bone, joint and knee) and soft tissue (skin, vascular graft, and ligament) are two big divisions of tissue applications. Many researchers have investigated soft tissue repair using biomaterial scaffolds on the basis of their function, restoration, and mechanical support [5].

Tissue engineering is a branch of knowledge that engineers the biological substance for tissue regeneration to maintain and improve tissue functions. The development of tissue engineering has been adapted to use biomaterial scaffolds to repair/replace the damaged tissue and to maintain the living tissue functions. The applications of the tissue engineering are very broad for different types of tissues in the body, and engineered tissues are designed basing on the requirement of the tissue/organs and the surroundings around the target organs. It has been shown that many researchers have different approaches for different types of tissues/organs such as skin, lung and cardiac tissues [6-9].

1.2 Nanostructured biomaterials for vascular regeneration

1.2.1 Vascular regeneration challenges

Cardiovascular diseases, including coronary and periphery vascular diseases, suffer more than one million of patients annually in USA [10]. Tissue engineering approaches become interesting for vascular graft development because it would eventually regenerate a native blood vessel itself. Synthetic vascular graft from biodegradable polymers, such as polylactide, poly(glycerol-sebacate), polycaprolactone and polyurethane, have been explore for the vascular regeneration and repair purpose

[11-15]. However, post-treatment of synthetic vascular graft has showed the negative down side which is intimal hyperplasia and thrombosis.

Intimal hyperplasia is an event that the vascular smooth muscle cells over-proliferate at the inner layer of the blood vessel wall. The cause of this occurrence come from many factors such as inflammation, injury and stretches [16]. The blood vessel comprise of 3 different layers which are intima, media and adventitia. In the intima layer, there are many crucial components such as endothelial layer, extracellular matrix and basement membrane [17]. The endothelial layer can be damaged by over population of vascular smooth muscle cells from 20% to 70-80% [18]. The damaged endothelial layer can induce the thrombus formation, which cannot inhibit the proliferation of the vascular smooth muscle cell at the normal level [19].

Thrombosis is process of thrombi or blood clots because of coagulation factor, fibrin and platelets. The blood vessel wall can be damaged due to the accumulation of the platelets and fibrin at the injured wall [20]. The breakdown formation of the thrombi follows by the thromboembolism lead to the cardiovascular diseases, such as myocardial infarction [21].

1.2.2 Vascular graft in biomedical application

Over 400,000 of heart bypass operation procedures using either autologous vein and arteries or vascular grafts were done annually. Interestingly, small diameter vascular grafts (< 6 mm in diameter) were often used in the surgeries due to the restoration of the small blood vessel. There are many types of vascular grafts developed over the past decades, and their result outcomes revealed the promising potential for vascular regeneration. However, it cannot meet the requirement of the ideal vascular graft. The ideal vascular graft requires nonthrombogenic, compatible at high blood flow rates, and

viscoelasticity match to native vessels. Many problems have been occurred from using vascular grafts in clinical trials such as compliance mismatch, thrombogenicity, poor haemodynamics, luminal narrow and intimal hyperplasia [22].

Polytetrafluoroethylene (PTFE) and Dacron are the prosthetic grafts which have been commonly used in clinic. PTFE is an inert fluorocarbon polymer which can be extruded into expandable polytetrafluoroethylene (ePTFE). This ePTFE has high crystallinity (90%), stiffness (0.5 GPa), and tensile strength (14.0 MPa). Therefore, ePTFE has been used for lower limb bypass grafts (7–9 mm) and revealed the promising results in large diameter replacement. However, ePTFE grafts show some degree of failures in small diameter vascular graft post-operations due to the thrombosis and intimal hyperplasia. The reason behind this phenomenon is the properties of ePTFE, which is non-biodegradable and electronegative luminal surface [23].

Dacron or poly (ethylene terephthalate) is a type of polyesters and has many techniques to form a vascular graft, including knitting and weaving. Dacron is non-biodegradable and has high tensile strength (170-180 MPa), tensile modulus (14,000 MPa), and crystallinity [24]. Dacron pore size can be tunable depend on the procedure of forming vascular graft such as small pore by weaving and large pore size by knitting. The pore size can be beneficial in tissue ingrowth but lack of blood hemodynamic in aorta.

PTFE and Dacaron are widely used for vascular graft replacement; however, the nature of these materials is synthetic and non-biodegradable, leading to various drawbacks such as mechanical mismatch and material induced chronic inflammation. Development of biodegradable polymers scaffolds has been recently investigated and applied in the vascular graft application. In terms of the main advantages of the biodegradable polymer scaffolds, the scaffold degradation is a key to perform the extracellular matrix replacement/remodeling . This process is affected by cells growth in

the appropriate environment on the surface/inside of the scaffolds. The most commonly biodegradable polymer, such as poly(glycolic acid) (PGA) and polycaprolactone (PCL) have been widely used in tissue engineering . They can be degrades by hydrolysis and enzymes. The ester bond of PGA can be hydrolyzed, and the degradable product, glycolic acid, can also be eliminate and metabolized [23]. To prove that biodegradable polymer is a great candidate for making vascular grafts, many researches have focused on the effects of biodegradable scaffolds to the cells. PGA scaffolds have been developed and revealed that their mechanical properties were lost when the smooth muscle cells produced collagen. During PGA scaffold degradation, the burst pressure of the vasuclar graft turned higher. Nevertheless, PGA scaffolds exhibit the endothelium layer formation is not completely presented. Moreover, the scaffold reacts to serotonin and endothelelin-1 which related to the endothelial formation [25].

Polycaprolactone (PCL) is another versatile polymer which has been used in tissue engineering. PCL reveals very slow degradation rate by the hydrolysis reaction of the ester bond with the elimination of macrophages and giants fragments. PCL based scaffolds made pf PCL-poly(lactic acid) copolymer have been studied about the smooth muscle cell and endothelial cell formation. The smooth muscle cell and endothelial cell formation was observed, but in some case, overpopulated growth of smooth muscle cells also were observed. To across this challenge, the drug load scaffold was considered to be used to overcome this limitation [26-27].

1.3 Nanostructured biomaterials for lung regeneration and repair

1.3.1 Lung regeneration and repair

Lung diseases like chronic obstructive pulmonary disease (COPD), and asthma are estimated to be the fifth major cause of death in 2020 worldwide [28]. The major

challenge to lung disease treatment is inflammatory response. Many approaches have been shown in the past decade such as pulmonary rehabilitation, noninvasive ventilation and pharmacological [29]. Pulmonary delivery has many benefits for lung treatment, for instance, non-invasive delivery and large surface for absorption. From late 1960s, nanoparticles start to be developed for drug delivery applications and continue until now. Sustained drug release, non-invasive drug delivery, drug entrapping in thin layer of lung epithelial cell, and avoiding the alveolar macrophages are the crucial advantages of using nanoparticles for pulmonary delivery to treat lung diseases [30]. Moreover, targeted delivery also showed the potential of reducing overall doses and side effects to the patients.

In order to improve the nanoparticle delivery to the lung, maximizing the nanoparticle deposit on the thin layer of lung epithelial still remains challenge. To overcome this challenge, surface modification on the surface of nanoparticle is an alternative approach to this problem. In fact, many types of nanoparticles have been widely investigated to solve this problem such as peptide, lipid and antibiotic incorporated with natural/polymeric based nanoparticle [31-35].

NP development in lung regeneration has been investigated, and both cDNA plasmids and proteins such as growth factors are commonly delivered to the lung for regeneration. Conventional delivery of proteins and DNAs has been revealed the huge drawbacks of bioavailability, denaturing/instability of the product and dose control. Therefore, nanoparticle delivery of the therapeutic agent by pulmonary delivery or inhalation has been investigated and proved the beneficial. The advantages of this methods are non-invasive, the large alveolar surface area for NP uptake, prolonged local action, and a lower effective dose.

1.3.2 Nanomaterial for delivery of therapeutic reagents

Nanoparticles have been widely used in delivery the therapeutic agents to the lung by pulmonary delivery. The reasons are located on the benefit of using nanoparticles, which are non-invasive, local delivery/action of therapeutic agent, availability of large alveolar surface area, and reduced systemic side effects due to site (lung)-specific delivery of encapsulated therapeutic agents. There are many types of nanoparticles which have been revealed in pulmonary delivery such as liposomes, micelles, and polymeric nanoparticles [36].

Liposome is a bilayer phospholipid vesicle which has hydrophilic core to load the hydrophilic therapeutic agents into the core. This type of nanoparticles are very attractive to deliver a therapeutic agent to the lung because of the similarity of the nanoparticle composition matching with the lung surfactants in the human body and the biocompatibility. However, the huge drawback of using liposome is the aggregation of the lipid itself [37].

Micelle is a single nano-size layer phospholipid carrier which comprises of a hydrophilic shell and hydrophobic core. The big advantage of the micelle is the capability to carry/delivery the varying solubility of the therapeutic agents. Moreover, the hydrophilic shell serves as a barrier to evade the reticuloendothelial system and avoid the fast elimination from lung administration. Although the high impact of micelles is promising, the drawbacks of micelles, which are the slow extravasation and chronic liver toxicity due to the slow metabolic process, cannot be neglected [38].

Polymeric nanoparticles have been extensively developed recently for the pulmonary drug delivery. The natural polymers used for synthesized nanoparticles are cellulose, chitosan, gelation, alginate, and others. The synthetic polymers such as PLGA,PCL, PLA and PGA are also used to make nanoparticles for drug delivery

applications. Degradation rate for each type of nanoparticles is the crucial factor for choosing the type of the polymer which affect the release profile of therapeutic agents [39].

1.4 Nanostructured biomaterials for skin regeneration and repair

1.4.1 Skin tissue regeneration and repair physiology

Chronic wounds, including burn and skin ulcers, have been reported over 7.5 million patients in the United State in 2011 [40]. In the past, traditional wound dressings, such as bandages, cotton wools, and gauzes, were developed for wound healing treatment. The key of wound dressing is to keep the wound dry to prevent any bacteria invasive into the wound injury [41]. However, the possible major problem come along with these traditional wound dressings is bacterial infection. Moreover, tradition wound dressing did not meet all the requirements of wound care which allow the great environment for healing process. It has been suggested that nanofiber can avoid the bacteria infection, and promote the environment for healing base on its properties which show highly porosity, gas permeation, surface area and great mechanical properties [40].

Wound healing is a process when the skin gets damaged and the body responds to that with complicate mechanisms. There are many types of wounds such as acute and chronic base on the healing time. Acute wound is a wound that the human body responds to and normally heals by itself. On the other word, chronic wound is a wound that halted in the inflammatory stage. Chronic wound healing takes longer time than acute wound healing which presents in high level of matrix metalloproteinases (MMPs). The high level of MMPs could cause extracellular matrix and growth factors degraded. The long process of wound healing affected the activity of the cell, especially skin fibroblast cells [40]. The wound healing process comprise of five stages, which are homeostasis, inflammation,

migration, proliferation and maturation stages [42]. Homeostasis stage is a stage that occurs in the first 15 minutes of skin injured and bleeding. The injured blood vessel is initiated to vasoconstriction to prevent the blood flowing in the local tissue, and to get rid of the antigen and bacteria from the wound. Thrombocytes and many other blood cells migrate to the injured area to form blood coagulation with fibrinogen. The inflammatory stage could prolong up to 6 days depending on the chronic level of the wound. The growth factors are produced in this stage by the polymorphonuclear cell, and this kind of cell can also get rid of the bacteria and foreign substances. Fibroblasts cells migrate to the injured area to proliferate and produce collagen stimulated by monocytes to thicken the epithelial layer under the clot, which is revealed in migration stages. After that, the granulation tissue forms, and the angiogenesis process takes place in the proliferation stage. The final stage of wound healing is maturation or remodeling stages, where the connective tissue and epithelium layer are formed [40-42]. In the future, we will focus on inflammatory, migration and proliferation phases which related to bacterial infection and skin fibroblast. The bacterial infections prolong or slow down the inflammatory stages and the movement of skin fibroblasts affects the epithelial thickening in the migration stage.

1.4.2 Nanomaterial as a skin grafts

Typical wound dressing usually play crucial roles as a temporary barrier for hemostasis and infection prevention purposes. In the past decades, skin graft was synthesized using natural and synthetic polymer to develop a wound dressing replacement applications [43]. Nonetheless, they have drawbacks, which include extensive care, do not regain full skin functionalities, and high cost. Therefore, a new type of wound dressing is taking into account by using natural and synthetic polymer to form a hydrogel. Hydrogel is an alternative choice for the wound dressing, which has the

benefits of maintaining moisture at wound site and capability of drug delivery. However, the non-degradable of the hydrogel itself and limitation of the diffusion process are the main challenges of using hydrogel in wound healing application as a wound dressing [44]. To date, there are many approaches to overcome these drawbacks of current wound dressing by incorporating the drug to accelerate the wound healing process and developing a new type of wound dressing via a nanofiber scaffold.

The scaffold has been widely used in tissue engineering application because of the benefit of the scaffold that has positive impacts in the treatment. Many researchers have revealed to deliver growth factors using scaffolds and nanofibers as a wound dressing. It has been proved that delivering growth factors helps the healing process and accelerates the cell proliferation. But the growth factors are easily degraded during the wound healing process which affects by proteinase [45]. Therefore, this approach has been limited by the cost of batch production and amount of growth factor delivery each time. Until now, current treatment methods cannot meet the requirements to achieve satisfaction of regaining barrier functionality and the acceleration of the wound healing process of natural skin. Thus, we expect that we can develop a new wound dressing with functions of both antimicrobials and growth factor release.

1.5 Overview of Research Project

This research project has been focus on the development of a new nanostructure biomaterial for treating various types of tissues for regeneration and repair purpose. The overall goals and specific aims of this project have been described in detail as below.

1.5.1 Goals and Objectives

Our overall goals are to explore and alleviate the current problems at various tissue organs such as vascular, lung and skin tissues. Briefly, we found out the problems of using artificial vascular grafts which are thrombosis, intimal hyperplasia, and endothelial formation. The current treatments are not able to solve these problems at the same time; therefore, we propose a new promising system that can overcome these limitations (aim 1). Moreover, lung disease is one of the most common chronic diseases which cause many deaths in a year. Inhalation drug delivery has been widely used to treat this disease; however, the lack of efficiency to deliver the therapeutic agents to the lung tissue is the major cause due to the drug concentration and side effects. Thus, we come up with the new design of nanoparticle to maximize the drug delivery efficiency by improving the NP cellular uptake, sustained-long term drug release for lung regeneration (aim 2). Last but not least, wound healing or skin repair is one the many applications that receives benefit from tissue engineering by developing biomaterials to prevent infection and promote tissue regeneration. Many of wound dressings have been shown the potential to prevent bacteria pathogen; however, they still lack of the efficiency to kill various types of bacteria pathogens significantly. Hence, we would like to present the new type of biomaterial incorporated with therapeutic agents which can kill various types of bacterial types significantly while supportting skin cell proliferation (aim 3).

1.5.2 Specific Aims

To achieve our goals of developing nanostructures biomaterials for tissue regeneration and repair, the following three specific aims have been proposed:

Aim 1: To develop an acellular biodegradable vascular graft which prevents thrombosis, inhibits smooth muscle cell growth and supports endothelial formation for

vascular regeneration. Polyurethane matrix with anti-thrombogenic drug (Dipyridamole) vascular graft was made via an electrospinning technique.

Aim 2: To develop an ECM-coated biodegradable nanoparticle for lung regeneration and cellular retention. Poly(lactic-co-glycolic acid) (PLGA) is chosen to fabricate nanoparticles coated with porcine lung extracellular matrix for maximizing NP cellular retention and uptake purposes.

Aim 3: Make conclusions and discuss future works. Furthermore, in terms of Aim 1 and Aim 2 results, we will preliminarily develop new wound dressing nanostructured materials. To develop an antimicrobial-nanofibrous scaffold for skin regeneration. Anti-microbial peptides and/or antibiotic drugs were incorporated with the polyurethane nanofibrous scaffold to prevent bacterial infection.

1.5.3 Innovation aspects

1.5.3.1 Aspect for Aim 1

The limitation of biodegradable vascular graft can be resolved by incorporating drug which has the properties to prevent thrombosis, inhibit smooth muscle proliferation and support endothelial formation into the system. Dipyridamole (DPA) is an anti-thrombogenic drug which prevents platelet activation/accumulation, inhibits proliferation of vascular smooth muscle cells and induces endothelial cell growth. We select biodegradable polyurethane (BPU) to be served as an artificial vascular graft due to great biocompatibility and mechanical properties. The drug-blended polymers nanofibrous scaffold vascular like can be done using an electrospinning technique. The drug will be released by diffusion and degradation of polymer mechanism to perform its functions.

1.5.3.2 Aspect for Aim 2

Surface modification of nanoparticle (NPs) has been proved to enhance the NP retention. Adapting this idea, we found out that extracellular matrix (ECM), which comprises of many substances including collagen, elastin, laminin, and proteoglycans, which play crucial roles in supporting diverse cell functions such as adhesion and proliferation. Moreover, many studies have shown that incorporation of ECM provides adhesive cues or integrin-binding sites for cell adhesion to the synthetic polymers. We hypothesized that ECM coating on the surface of NPs could enhance the adhesion interactions between nanoparticles and lung epithelial cells, which could improve the NP uptake and cellular retention. Therefore we developed a ECM-coated biodegradable NPs to enhance cellular uptake/retention and maximize the therapeutic delivery for lung tissue regeneration purpose.

1.5.3.3 Aspect for Aim 3

On the basis of Aim 1 and Aim 2, we will make solid conclusion, set up the future work, and collecting preliminary resutls in developing new nanostructured scaffolds for skin regenration and wound healing. Antibacterial nanofibers have been researched and shown the promising approach for wound healing application. However, it did not answer or cover all the aspects, including to promote great environment for healing process. Bacterial invasion, resistance, and cell interaction are the main problems need to be managed. Therefore, nanoparticle incorporated with anti-microbial loaded into nanofibers and antibiotics release combination could be a great strategy to take care of these issues simultaneously.

1.5.4 Successful Outcome

The successful outcome of this project will provide a new generation of nanostructured biomaterials to be used in vascular, lung and skin regeneration and repair. Development of biodegradable scaffolds for vascular which overcome the current problems such as intimal hyperplasia and endothelial formation has been done and revealed. It is crucial to implement vascular graft problem to prolong patient life. Since each organ has its own complication, the development strategies of a new nanostructured biomaterial are not fixed. To further our investigation, new types of pulmonary nanoparticle delivery for lung regeneration has been successfully fabricated. This is very important to accelerated and achieve the lung regeneration purpose. Moreover, the knowledge gain from these studies is enormous according to the variety of biomaterials and types of organs for tissue regeneration. In addition, improve the quality of life and prolong the patient's life are the outcomes that we are looking for.

Chapter 2

Development an electrospun nanofibrous scaffold for vascular regeneration

2.1 Introduction

Approximately 80 million patients suffer annually from cardiovascular diseases, including coronary artery and peripheral vascular diseases, in the USA alone [46]. Replacing diseased or narrowed blood vessels is the most effective treatment for the vascular diseases. Artificial vascular grafts are the best substitution to vein grafts to solve the problem of limited vein graft resources. Large diameter vascular grafts (>6 mm inner diameter) from non-degradable polymers, such as Dacron and polytetrafluoroethylene (PTFE), have achieved great clinical success. However, PTFE and Dacron failed in small diameter vascular graft ($\leqslant$6 mm inner diameter) applications due to stenosis [47].

Biodegradable small diameter vascular grafts (SDVGs) are attracting increasing interest in vascular tissue engineering because they have the potential to eventually regenerate blood vessels similar to those of patients. The SDVG is implanted directly into the patient without cell loading. It requires cellular ingrowth from native tissues along with material degradation, then eventually forms a functional vascular replacement. The SDVGs prepared from biodegradable synthetic polymers, such as polylactide [48] and [49], poly(glycerol sebacate) [50], polycaprolactone [51] and polyurethane [52-53], have been investigated for this purpose. However, the implanted material would induce acute thrombosis and intimal hyperplasia (IH, smooth muscle cell over-proliferation), which are two major barriers to the biodegradable SDVGs. Additionally, rapid and adequate endothelialization on the graft lumen is the major key to achieving long-term SDVG patency. Thus acellular biodegradable SDVGs need to be capable of preventing thrombosis and IH, as well as promoting rapid endothelialization.

Many approaches have been utilized to improve the blood compatibility and IH inhibition of acellular SDVGs. Those include surface modification [54-56], polymer composition modification [53] and [57], nitric oxide release [58-60] and drug release [61-63]. Of these strategies, the drug release approach is an easy way to improve the biofunctions of biodegradable polymers. For example, antiproliferative paclitaxel release from polycaprolactone contributed to the inhibition of smooth muscle cell (SMC) proliferation to achieve a high patency *in vivo* [63]. However, the paclitaxel incorporation cannot meet all the required factors for vascular grafts, such as rapid endothelialization, as this drug markedly delays endothelial cell (EC) layer formation. Dipyridamole (DPA), which is an antithrombogenic drug used clinically, can reduce SMC proliferation by inhibiting adenosine uptake and cyclic nucleotide phosphodiesterase activities in cells, resulting in the intracellular increase of cAMP and cGMP levels [64-68]. In particular, it was also reported that the DPA promoted vascular endothelial cell proliferation [64, 67]. Thus, combining the versatile DPA with a biodegradable polymer would be a solution to overcome the limitations of current strategies, such as paclitaxel-loaded vascular prostheses.

Our aim in this work is to fabricate a biodegradable scaffold with multiple biofunctions as an acellular SDVG by combining a drug with a biodegradable polymer. A biodegradable elastic polyurethane and the multifunctional drug DPA were mixed and electrospun into fibrous scaffolds. The BPU would provide temporary mechanical support matched to that of native blood vessels, with sufficient mechanical strength to withstand surgical handling. The DPA in the scaffold would be released and provide biofunctions, including antithrombosis, SMC proliferation inhibition and EC proliferation stimulation. The morphology, mechanical properties and shrinkage of the DPA-loaded BPU scaffolds were evaluated. The long-term drug release kinetics was measured under physiological

conditions. Human blood was used to evaluate the scaffold's hemocompatibility through blood clotting, hemolysis and platelet deposition tests. Proliferation of human aortic smooth muscle cells (HASMCs) and human aortic endothelial cells (HAECs) with the scaffolds was assessed *in vitro*.

2.2 Experiment section

2.2.1 Materials used

Polycaprolactone diol (PCL, Mn = 2,000, Sigma, St. Louis, MO) was dried in a vacuum oven at 60^{o}C overnight before use. Putrescine (Sigma) and hexamethylene diisocyanate (HDI; Sigma) were purified by distillation. Stannous octoate (Sn(Oct)2; Sigma) was dried by passing through a 4 Å molecular sieve. DPA (Sigma), anhydrous dimethyl sulfone (DMSO; Sigma), isopropanol (Sigma) and 1,1,1,3,3,3-hexafluoro-2-propanol (HFIP; Oakwood Products) were used as received. Other chemicals were purchased from Sigma, unless otherwise specified.

2.2.2 Synthesis of BPU

BPU was synthesized using a modification of a protocol described previously [69]. Briefly, PCL was dissolved in DMSO in a three-necked flask with nitrogen protection, then HDI and three droplets of the catalyst Sn(Oct)2 were added. After 3 h at 70 °C, the mixture was cooled down to room temperature. A putrescine/DMSO solution was then added to the flask with agitation. The molar ratio of PCL/HDI/putrescine was 1:2:1, and the final polymer concentration in the flask was around 4% (w/v). The flask was kept at 70 °C overnight, whereafter the polymer was precipitated in deionized water. The obtained polymer was rinsed three times in a large amount of water, then immersed in

isopropanol to further remove unreacted monomers and oligomers. Then the obtained BPU was dried in a vacuum oven at 60 °C for 3 days. The yield was above 85%.

2.2.3 Fabrication of electrospun drug-loaded nanofibrous scaffolds

BPU and DPA were mixed and dissolved in HFIP at DPA concentrations of 0, 2.5, 5 and 10% to BPU. The BPU concentration was 6% (w/v) in the solution. The mixed solution was loaded into a 10 ml syringe connected to a stainless steel capillary. The capillary was charged with a high voltage of 12 kV, and a conductive metal collector covered with an aluminum foil was charged at −10 kV. The distance between the capillary tip and the collector was 30 cm. The collector was rastered at a speed of 5 cm s–1 on both the x and y axes (Velmex Inc., USA). The mixed solution was electrospun vertically at a flow rate of 1 ml h–1. After 4 h, the electrospun sheets were removed from the foil and dried overnight in a vacuum desiccator for further use. The resulted scaffolds containing 0, 2.5, 5 and 10% DPA were named as BPU, BPU+2.5% DPA, BPU+5% DPA and BPU+10% DPA, respectively.

To fabricate a small diameter conduit, a 2 mm outer diameter mandrel, used as a collector, was rotated at a 100 rpm speed and rastered at a speed of 2 cm s–1 on the x axis. The other conditions were the same as above. After 1 h, the conduit were removed from the mandrel and placed in the vacuum desiccator for further imaging.

2.2.4 Scaffold characterization

The electrospun sheets and conduits were sputter-coated with silver and their surface morphology was then observed using a scanning electron microscope (SEM; Hitachi, S-3000N). The fiber diameter was measured using software ImageJ (National Institutes of Health).

For the uniaxial tensile mechanical properties, a 2 × 20 mm strip cut from the electrospun scaffold was measured at a crosshead speed of 10 mm min–1 with a 500 N loading cell at room temperature on an MTS Insight workstation (MTS system corporation, MN) according to ASTM D638-98.

For the suture retention strength [70], a 5 × 20 mm strip was cut from the electrospun scaffolds. A loop of suture (4-0 silk black braided, Ethicon) was fabricated at 5 mm from one end of the strip. The sample was then tested on an MTS Insight workstation under the same conditions as the above tensile test. The suture retention strength was calculated as load force (N)/(suture diameter (mm) × sample thickness (mm)).

For the shrinkage, a disk sample (D0 = 6 mm diameter) was punched from the electrospun scaffold using a standard biopsy punch (Miltex, PA), then immersed into phosphate buffer solution (PBS) at 37^{o}C for 24 h. The sample diameter was then measured (D1) using a sliding caliper. The shrinkage ratio was calculated as (D0 − D1)/D0 × 100%. The sample morphology was observed in an SEM and the fiber diameter was measured using ImageJ. The mechanical properties of the samples after PBS immersion were measured as described above.

2.2.5 In vitro drug release kinetic

The weighted nanofibrous scaffold (4–6 mg) was immersed in 10 ml PBS at pH 7.4 under a sink condition (DPA solubility 0.922 mg ml–1 in water) in 20 ml vials. Each vial was then placed into an orbital shaker at 37 °C. At each time point, 1 ml of buffer solution was collected and kept at −20 °C for future analysis, then 1 ml of fresh PBS was added. The DPA released into the PBS was quantified by detecting fluorescence intensity. Briefly, 100 µl of collected buffer solution and 100 µl of 100% ethanol were

mixed in a well of a 96-well plate. The fluorescence intensity was then recorded at 295 nm (excitation) and 485 nm (emission) on a UV/vis spectrophotometer (Infinite M-200, Tecan) [71]. A standard curve was performed using a series of known DPA contents in 50% ethanol/PBS solution. As a control, BPU alone was immersed in PBS at 37 °C and the fluorescence intensity of the collected solution was detected as described above up to 21 days. The morphology of the sample 91 days after release was observed using an SEM.

2.2.6 In vitro human blood tests

The process used to collect and handle human whole blood was approved by the Institutional Review Board (IRB) at the University of Texas at Arlington. Human whole blood was drawn by venipuncture and then transferred to anticoagulant tubes containing trisodium citrate, citric acid and dextrose.

The disk sample (6 mm diameter) was sterilized under UV irradiation for 1 h, rinsed three times using PBS and then placed into a 2 ml plastic centrifuge tube to measure the blood clotting time. For this, 0.85 ml of calcium chloride solution (0.1 M) was mixed with 8.5 ml of anticoagulated blood, then 50 µl of the blood with calcium chloride was added to the tube. At each time point (10, 20, 30 and 40 min), 1.5 ml of distilled water was added to the tube. After 5 min of incubation, images were taken by a digital camera. Next, 200 µl of the lysate was collected and its absorbance was measured at 540 nm using a UV/vis spectrophotometer [72].

A sterilized 6 mm diameter disk was placed in a 1.5 ml plastic centrifuge tube for hemolytic evaluation. A 5% diluted anticoagulant blood solution was prepared by mixing the whole blood with saline solution (0.9% NaCl solution). Next, 200 µl of diluted blood solution was added to the tube. After 2 h incubation at 37 °C, the tube was centrifuged at

1000g for 10 min. The supernatant was collected and transferred into a 96-well plate to measure the absorbance at 545 nm using an UV/vis spectrometer [73]. A negative control was prepared by adding 200 µl of anticoagulated blood in 10 ml of saline solution, and a positive control was obtained by adding 200 µl of anticoagulated blood in 10 ml of distilled water.

The concentration of thrombin–antithrombin (TAT) complex was measured to quantify thrombin formation. A 6 mm diameter sterilized sample was immersed in 1 ml of human whole blood at 37 °C for 1 h in a 2 ml plastic centrifuge tube. The tube was then centrifuged at 4000 rpm for 15 min to obtain platelet-poor plasma (PPP) [74]. The concentration of the TAT complex in PPP was detected using an ELISA kit (Assay Pro, MO) following the manufacturer's protocol.

Human blood platelet deposition on the scaffold surface was measured using human platelet-rich plasma (PRP), which was produced by centrifuging the human whole blood at 250g for 15 min [75]. A 200 µl aliquot of PRP was added to the surface of a sterilized scaffold sample (6 mm diameter) in a 48-well plate. After incubation at 37 °C for 1 h, the sample was then rinsed three times using PBS. The platelets deposited on the scaffold were quantified using a lactate dehydrogenase (LDH) assay following the manufacturer's instructions. To observe the blood platelet morphology, the PRP-treated samples were fixed in 2.5% glutaraldehyde solution for 2 h, then stained using 1% osmium tetroxide solution for 1 h. After dehydrated using a series of ethanol solutions (50, 75, 95 and 100%) for 15 min at each step and 100% hexamethyldisilazane (HMDS) for 30 min, the samples were dried in a desiccator, sputter-coated with silver and then observed under an SEM.

2.2.7 Human aortic smooth muscle cells (HASMCs) proliferation inhibition

HASMCs (ATCC, Manassas, VA) were seeded at a density of 2000 cells per well, then cultured overnight using Ham's (Kaighn's) Medium (F-12 k) supplement with 10% fetal bovine serum (Thermo Scientific, MA) and penicillin–streptomycin (100 U ml–1) (Life Technologies, CA). Scaffolds (6 mm in diameter) were then placed in the culture medium in each HASMCs-preseeded well. The cells continued to be cultured for 7 days. The culture medium was exchanged every 2 days. Tissue culture polystyrene (TCPS) without treatment was used as a control. Cell viability was assessed using an MTT assay (Sigma, MO) at each time point (1, 3, 5 and 7 days) following the manufacturer's instructions. Briefly, 20 μl of 3-(4,5-dimethylthiazol-2-yl)-2,5-diphenyltetrazolium bromide solution (5 mg ml–1) was added to each well and incubated for 4 h. The solution and the samples were then removed and 200 μl of DMSO was added to dissolve the blue crystal. The absorbance was detected at 570 nm using a UV/vis spectrophotometer. The cell viability was normalized by setting the absorbance of the control TCPS at day 1 as 100%. The cellular morphology was observed using a fluorescence microscope (Nikon Eclipse Ti, NY) after the cells had been stained using a live (calcein AM)/dead (ethidium homodimer-1) viability cytotoxicity kit (Life Technologies, CA).

2.2.8 Human aortic endothelial cells (HAECs) growth

HAECs (ATCC, Manassas, VA) were seeded in a 96-well cell culture plate at a density of 2000 cells per well and cultured overnight using endothelial basal medium (EBM-2) with endothelial cell growth media kits (EGM-2 bulletkit, Lonza, MD). The scaffolds (6 mm in diameter) were then placed directly in the culture medium in each HAEC-preseeded well. The cell culture medium was exchanged every 2 days. The TCPS without treatment was used as a control. At each time point (days 1, 3, 5 and 7), the cell

viability was measured using an MTT assay and a live/dead staining was performed to observe cellular morphology as described above.

In addition, HAECs were seeded on the scaffold surface to evaluate cellular accommodation. For this, 2000 cells were seeded on the surface of a 6 mm diameter disk scaffold and cultured up to 7 days. The cell culture medium was fully refreshed every 2 days. TCPS was used as a control. The cell viabilities at days 1, 3, 5 and 7 were measured using an MTS assay (Promega, WI). For cellular morphology, 10,000 cells were seeded on a scaffold surface and cultured up to 7 days. At each time point, the cell-seeded sample was fixed in a 2% glutaraldehyde solution, stained using 1% osmium tetroxide solution for 1 h and then dehydrated using a series of ethanol solutions (50, 70, 95 and 100%) for 10 min at each step. Further dehydration was conducted using a series of ethanol/HMDS solutions (2:1, 1:1 and 1:2) for 15 min at each step, followed by HMDS addition and evaporation. Finally, the cell morphology on the scaffold surface was observed under an SEM after silver coating.

2.2.9 Statistical analysis

All data were presented as mean ± standard deviation. Statistical analysis was performed using one-way analysis of variance with LSD post hoc test by Statview software. Four samples per group were used for our studies if no specified ($n = 4$). A statistical level of $p < 0.05$ was considered to be a significant difference.

2.3 Results

2.3.1 Scaffold characterization

A nanofibrous vascular conduit was fabricated by electrospinning a mixture of BPU and DPA, and appeared yellow because of the fluorescence intensity of DPA (Figure 2.1A). It was approximately 6 cm in length, with a 1.5 mm inner diameter and an

approximately 150 µm wall thickness (Figure 2.1 B and C). The electrospun nanofibrous sheet of each scaffold was continuous without beads in SEM images (Figure 2.2). The fiber diameters of the scaffolds ranged from 520 ± 100 to 650 ± 160 nm (Table 2.1).

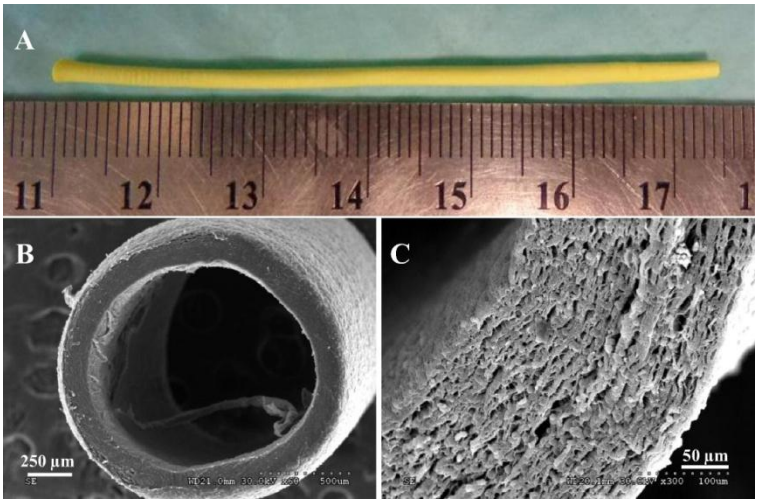

Figure 2.1: (A) A macroscopic view of a small diameter conduit from a mixture of BPU and 10% DPA to BPU by electrospinning. **(B and C)** Electronic cross-section images of the conduit.

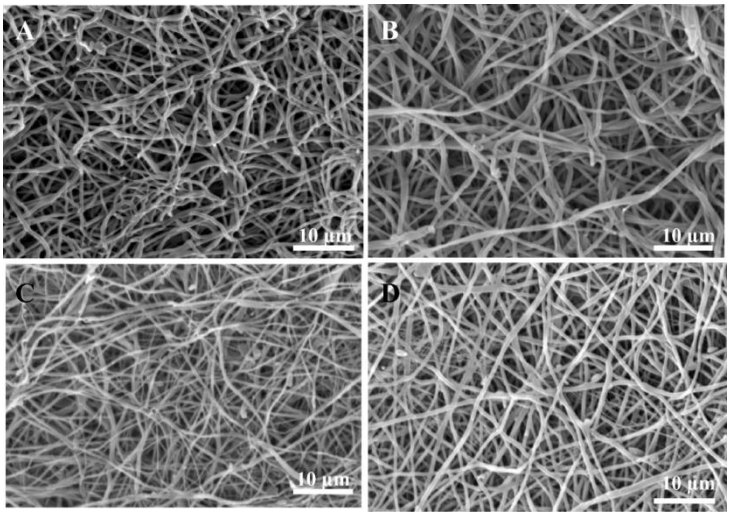

Figure 2.2: Micrographic fiber morphologies of **(A)** BPU, **(B)** BPU+2.5% DPA, **(C)** BPU+5% DPA and **(D)** BPU+10% DPA.

Table 2.1: Scaffold mechanical properties before and after 24 h PBS immersion.

	Before					After			
Samples	Fiber diameter (nm)	Stress (MPa)	Strain (%)	Initial modulus (MPa)	Suture retention strength (N/mm^2)	Fiber diameter (nm)	Stress (MPa)	Strain (%)	Initial modulus (MPa)
BPU	650 ± 160	3.4 ± 0.4	227 ± 30	1.4 ± 0.3	115 ± 35	570 ± 137	2.3 ± 0.5	180 ± 40	1.4 ± 0.5
BPU+2.5%DPA	610 ± 140	4.9 ± 1.2	130 ± 4	2.4 ± 0.4	69 ± 11	540 ± 124	4.4 ± 0.4	150 ± 16	1.6 ± 0.2
BPU+5%DPA	570 ± 110	5.7 ± 0.6	101 ± 14	3.5 ± 0.6	84 ± 17	500 ± 111	4.4 ± 0.7	106 ± 16	1.9 ± 0.4
BPU+10%DPA	520 ± 100	7.4 ± 0.1	107 ± 20	7.0 ± 1.0	98 ± 15	488 ± 72	6.2 ± 0.9	117 ± 18	2.8 ± 0.8

The mechanical properties of the scaffolds are listed in Table 2.1. The table shows a trend of increasing the uniaxial stress with an increase in DPA content in the scaffolds. BPU+10% DPA had the highest stress (7.4 ± 0.1 MPa), whereas BPU had the lowest stress (3.4 ± 0.4 MPa). The strains of all scaffolds were higher than 100%. The

initial moduli of the DPA-loaded BPU scaffolds were higher than that of BPU (1.4 ± 0.3 MPa). The BPU+10% DPA scaffold (7.0 ± 1.0 MPa) had the highest initial modulus. The suture retention strengths of BPU, BPU+2.5%DPA BPU+5% DPA and BPU+10% DPA are 115 ± 35 MPa, 69 ± 11 MPa, 84 ± 17 MPa, and 98 ± 15 MPa respectively.

The contraction of the DPA-loaded BPU scaffolds was clearly observed after 24 h of immersion in PBS at 37°C. As shown in Figure 2.3A, BPU scaffold had the lowest shrinkage ratio (0.6 ± 0.3%), while BPU+10% DPA had the highest (6.3 ± 0.4%). The shrinkage ratio of the scaffolds increased with increasing amount of DPA in the scaffold. Compared to the scaffold morphology before PBS immersion (Figure 2.2), the surfaces of all fibrous scaffolds became rougher with more coiled fibers (Figure 2.3B–E). Compared to the scaffold mechanical properties before PBS immersion, the stresses of all scaffolds except for BPU+2.5% DPA after PBS immersion significantly decreased, while the initial moduli of the DPA-loaded scaffolds significantly reduced after PBS immersion (Table 2.1). The initial modulus of BPU+10% DPA decreased from 7.0 ± 1.0 to 2.8 ± 0.8 MPa after PBS immersion.

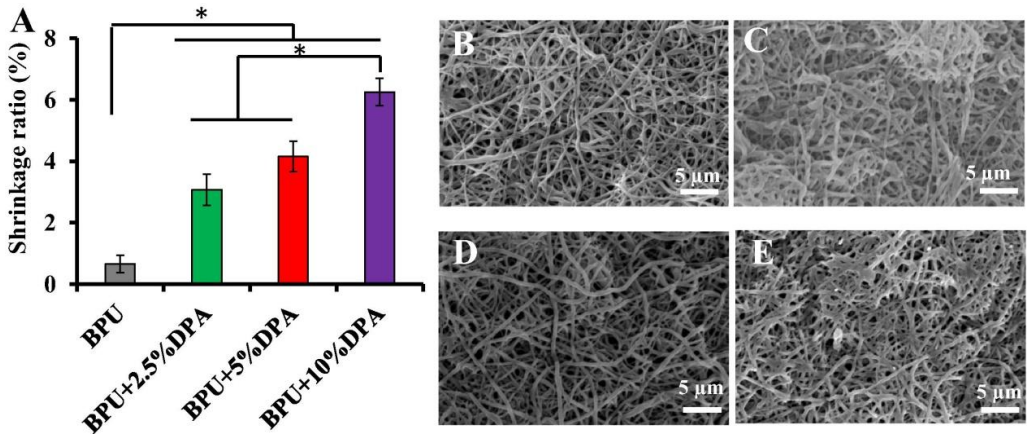

Figure 2.3: (A) Shrinkage ratios of electrospun scaffolds and micrographic fiber morphologies of **(B)** BPU, **(C)** BPU+2.5% DPA, **(D)** BPU+5% DPA and **(E)** BPU+10% DPA after 24 h PBS immersion at 37°C.

2.3.2 In vitro drug release kinetic

DPA release curves are shown in Figure. 2.4A. No obvious burst release was observed for the DPA-loaded BPU scaffolds within the first 24 h. The scaffolds had a faster release within the first 3 days, which changed to a slow release up to 91 days. The DPA release profiles of BPU+2.5% DPA and BPU+5% DPA did not show any significant difference ($p > 0.05$), but they were significantly faster than that of BPU+10% DPA ($p < 0.05$). At 91 days, BPU+10% DPA had cumulatively released 24 ± 3% drug, which was markedly lower than the BPU+2.5% DPA (64 ± 11%) and BPU+5% DPA (56 ± 12%). The scaffolds maintained a fibrous morphology beyond 91 days after release (Figure 2.4B–D). Some broken fibers were clearly visible for BPU+10% DPA (Figure 2.4D), while no fiber breakage was found for BPU+2.5% DPA (Figure. 2.4B) or BPU+5% DPA (Figure. 2.4C).

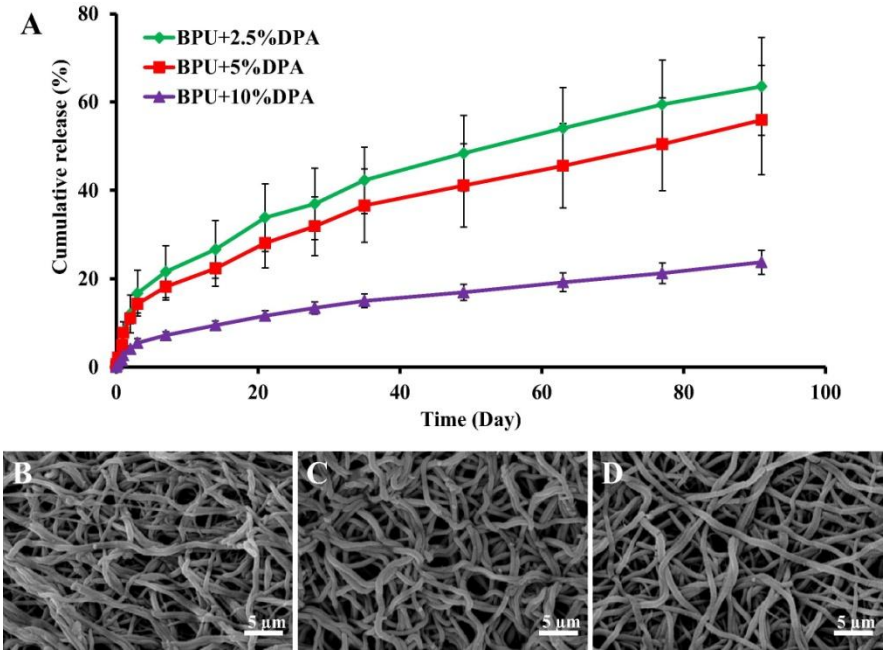

Figure 2.4: (A) In vitro DPA release curves of DPA-loaded BPU scaffolds up to 91 days in PBS at 37^{o}C. SEM images exhibited fiber morphologies of **(B)** BPU+2.5% DPA, **(C)** BPU+5% DPA and **(D)** BPU+10% DPA after 91 day release.

2.3.3 In vitro human blood test

Blood clot time was measured by observing clot formation at a series of time points. As shown in Figure 2.5A, human blood alone did not show any blood clot up to 20 min, though a slight clot at 30 min and a complete clot at 40 min were observed. For BPU, a slight blood clot was observed at both 10 and 20 min, and a complete blood clot was seen at both 30 and 40 min (Figure 2.5B). For BPU+10% DPA, the blood clot occurrence was similar to that of the blood alone (Figure 2.5C).

The blood clot time was detected by measuring the absorbance of the lysate solution. In Figure 2.5D, at 30 min, the absorbances for BPU+5% DPA and BPU+10% DPA were similar to that for the blood control ($p > 0.05$). In addition, in Figure 2.5E, BPU alone has the highest TAT complex concentration ($p < 0.05$). The TAT complex concentrations for the DPA-loaded BPU scaffolds were similar to the blood control ($p > 0.05$).The hemolysis percentages of all scaffolds were lower than 1% (Figure 2.5F). The hemolysis for BPU was the highest ($p < 0.05$), whereas BPU+5% DPA and BPU+10% DPA had the lowest hemolysis percentages ($p < 0.05$).

Human PRP was used to measure the platelet deposition on scaffold surfaces. In Figure 2.6A, blood platelet aggregations were clearly observed on the BPU surface. There were few platelet aggregations and individual platelets were sparsely distributed on the surface of BPU+2.5% DPA (Figure 2.6B). On the BPU+5% DPA surface, platelet aggregation and a few individual round platelets were visualized (Figure 2.6C). For BPU+10% DPA, few blood platelets with a round shape existed, whereas no platelet aggregation or spread was observed (Figure 2.6D). The number of platelets deposited was quantified using an LDH assay (Figure 2.6E). The platelet numbers on the surfaces of the DPA-loaded BPU scaffolds were significantly lower than on BPU.

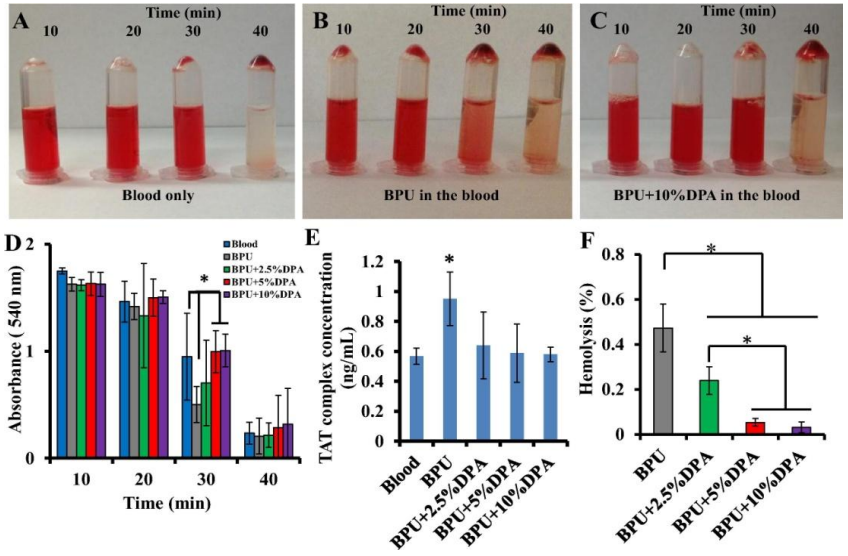

Figure 2.5: Digital images to show human blood clot formation with time of **(A)** human blood, **(B)** BPU alone in the human blood and **(C)** BPU+10% DPA in the human blood. **(D)** The absorbance at 540 nm of the lysate of human blood contacted with the scaffold. **(E)** The TAT complex concentration in PPP after the scaffold has been in contact with human blood. The control is human blood alone. **(F)** Human blood hemolysis percentages of the scaffolds.

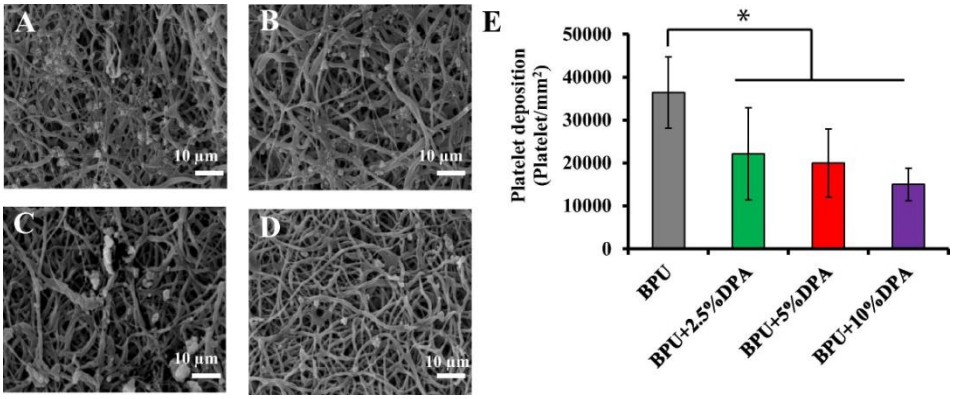

Figure 2.6: Human blood platelet depositions on the surfaces of **(A)** BPU, **(B)** BPU+2.5% DPA, **(C)** BPU+5% DPA and **(D)** BPU+10% DPA. **(E)** Quantification of human blood platelet deposition on the scaffold surfaces using an LDH assay.

2.3.4. In vitro HASMC proliferation inhibition

HASMCs on the TCPS and with the BPU did not proliferate at days 1 and 3, although higher cellular viability was seen at day 7 compared to day 1 ($p < 0.05$) (Figure 2.7). The HASMC viability did not show any significant difference between the DPA-loaded BPU scaffolds within 7 days of culture. From day 1 to day 3, there was no significant difference in cellular viability between all samples. At day 5, the HASMC viabilities for BPU+5% DPA and BPU+10% DPA were lower than that for TCPS ($p < 0.05$), and the cellular viability for BPU+10% DPA was lower than that for BPU ($p < 0.05$). At day 7, the HASMC viabilities for BPU+5% DPA and BPU+10% DPA were significantly lower than those for the TCPS control and BPU ($p < 0.05$). The cellular viability for BPU+2.5% DPA was lower than that for the TCPS control at day 7. In addition, in Figure 2.8, no dead cells (red dot) were visible. For TCPS (Figure 2.8A) and BPU (Figure 2.8B), HASMC confluence was clearly observed at day 7. For the DPA-loaded BPU scaffolds, HASMCs were sparsely dispersed on the culture plate surface, with little spread (Figure 2.8C–E).

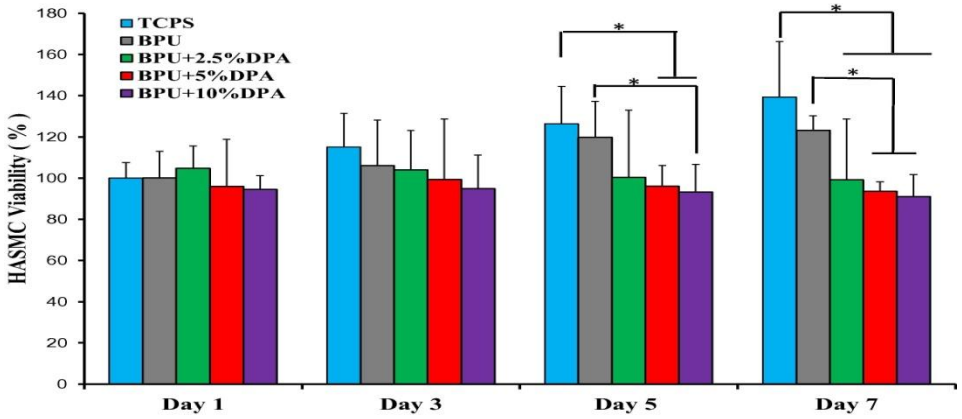

Figure 2.7: HASMC proliferation inhibition was evaluated using an MTT assay after incubating BPU and DPA-loaded BPU scaffolds in HASMC-preseeded wells. TCPS without any treatment was set as the control.

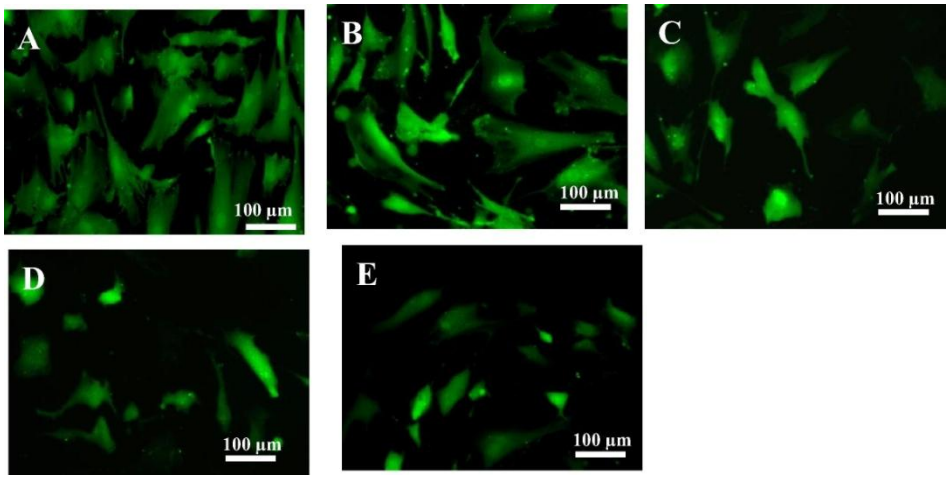

Figure 2.8: Live/dead staining to show HASMC morphologies on **(A)** TCPS and after incubating **(B)** BPU, **(C)** BPU+2.5% DPA, **(D)** BPU+5% DPA and **(E)** BPU+10% DPA in HASMC-preseeded wells at day 7. Green: living cells; red: dead cells.

2.3.5. In vitro HAEC growth

HAEC growth with DPA-loaded BPU scaffolds was evaluated using an MTT assay. In Figure 2.9, the HAEC proliferation with culture time is presented for all scaffolds and the TCPS control. The cell viabilities for the DPA-loaded BPU scaffolds were higher than those for the TCPS at days 3, 5 and 7 ($p < 0.05$). The cellular viability for BPU+5% DPA was higher than for BPU at day 7 ($p < 0.05$). For BPU+10% DPA, the cell viabilities were significantly higher than those for BPU at days 3, 5 and 7 ($p < 0.05$). Additionally, no dead cells were observed for all samples at day 7 (Figure 2.10).

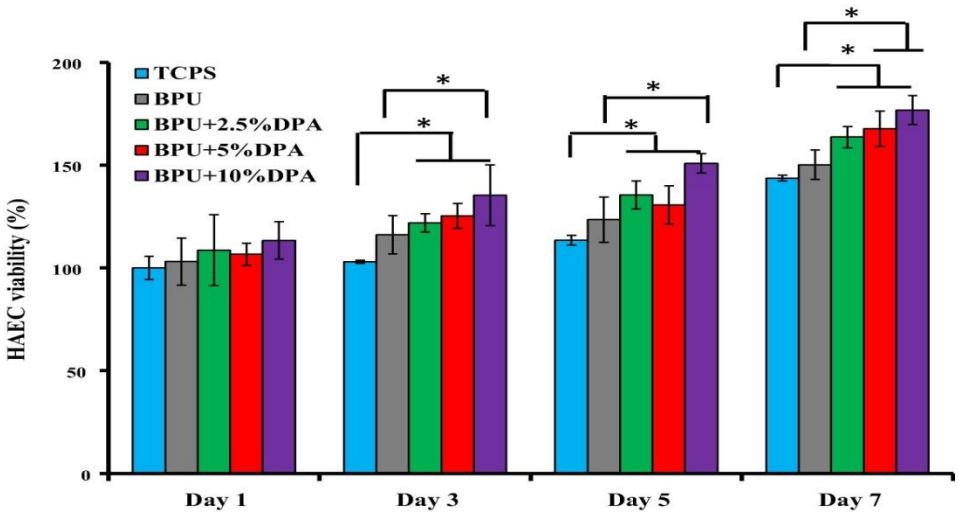

Figure 2.9: HAEC proliferation was assessed using an MTT assay after placing BPU and DPA-loaded BPU scaffolds in HAEC-preseeded wells. TCPS without any treatment was used as the control.

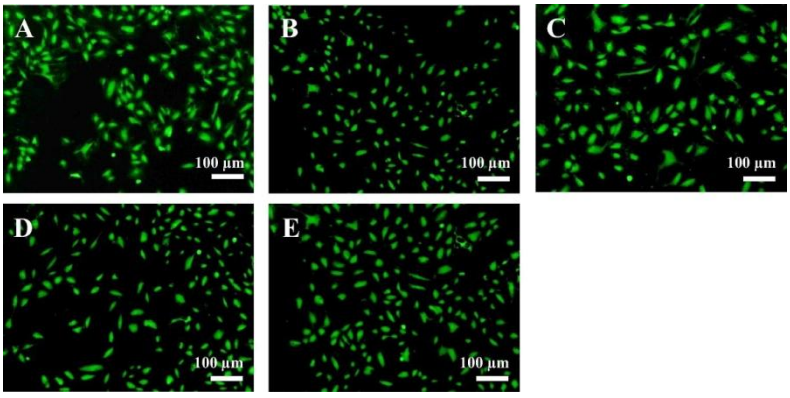

Figure 2.10: Live/dead staining to show HAEC morphologies on **(A)** TCPS and after incubating **(B)** BPU, **(C)** BPU+2.5% DPA, **(D)** BPU+5% DPA and **(E)** BPU+10% DPA in HAEC-preseeded wells at day 5. Green: living cells; red: dead cells.

HAECs were seeded on the scaffold surfaces to evaluate the cellular accommodation. In Figure 2.11A, no significant difference can be seen between the TCPS and DPA-loaded BPU scaffolds from day 1 to day 5, except for BPU+2.5% DPA at day 5. The cellular viabilities for BPU+10% DPA were higher than those for BPU at days 3 and 5. HAECs on the TCPS had the highest cellular viability at day 7 ($p < 0.05$). The cellular viabilities for BPU+5% DPA and BPU+10% DPA were significantly higher than that for BPU at day 7 ($p < 0.05$). Furthermore, spread HAECs and some spherical cells were observed on all scaffold surfaces at day 7 (Figure 2.11B–E). Especially for BPU+10% DPA at day 7, more spread cells and many spherical cells were observed (Figure 2.11E).

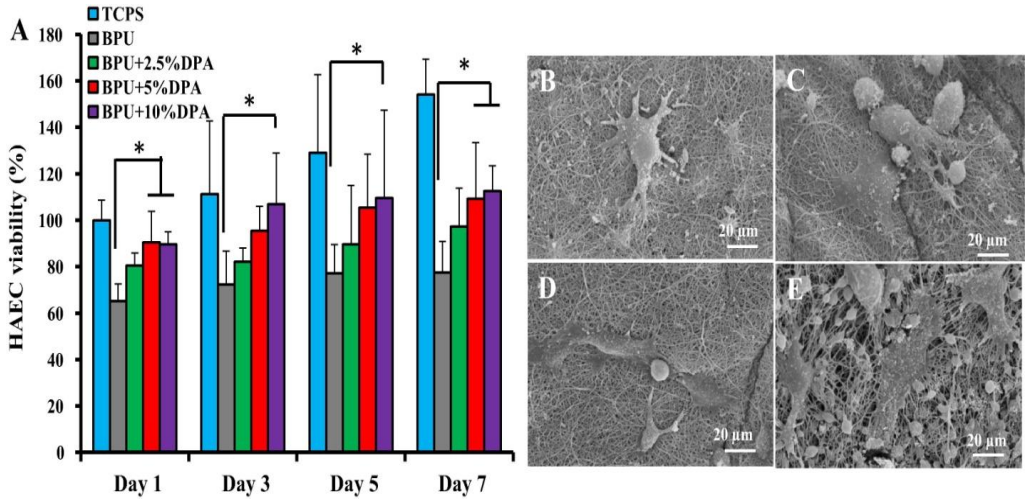

Figure 2.11: HAEC growth on the surfaces of BPU and DPA-loaded BPU scaffolds up to 7 days **(A)**. The TCPS surface served as the control. SEM images showed HAEC morphology on the surfaces of **(B)** BPU, **(C)** BPU+2.5% DPA, **(D)** BPU+5% DPA and **(E)** BPU+10% DPA at day 7.

2.4 Discussion

Small diameter vascular graft revealed the major issue in long-term thrombosis and restenosis. Incorporate dug into scaffold to overcome these limitations is a one way to do it such as heparin blended heparin, aspirin and paclitaxel incorporated with into biodegradable scaffold. Base on this advantages, DPA mixed with BPU and electrospun into a fibrous scaffold in this work. The released DPA could prevent thrombosis and inhibit SMC proliferation while improving endothelial cell growth. To our knowledge, the combination of DPA and a biodegradable SDVG has not been reported yet.

The reason of choosing BPU as a matrix material because it has good mechanical properties and biocompatibility. Previous studies have shown that this material can be processed into a conduit scaffold having compliance matching that of native artery. It has been show that mechanical properties and degradation can be tuned by altering the chemical components. Moreover, biofunctional and bioactive agents are capable of being incorporated with BPU via chemistry and engineering approaches . Its good biocompatibility has been verified from in vitro cell culture and in vivo implantation. PU-based scaffolds have been used to replace various tissues, such as blood vessels, myocardium, abdominal wall and bone.

Mechanical properties and its characterization

Mechanical propertied of the scaffold was affected by the incorporation of drugs into vascular grafts. Therefore, it is crucial to investigate these properties after drug loading. The DPA-loaded BPU scaffolds (dry state) were stronger and stiffer than BPU (Table 2.1). This may be a result of the enhanced hydrogen bonding between BPU and DPA because BPU contains urethane and urea groups (Fig 2A) and the small DPA molecule contains four hydroxyl groups and many nitrogen atoms (Fig 2B). The strong

interaction from hydrogen bonding is a double-edged sword. This interaction simultaneously increases the mechanical strength and the initial modulus of the scaffolds. The increase in the mechanical strength would strengthen the vascular grafts. However, the increase in the initial modulus may reduce the graft compliance and lead to a compliance mismatch with the native blood vessel. We noticed that, after PBS immersion, the stresses and the initial moduli of hydrated scaffolds (wet state) were significantly lower than those of scaffolds in the dry state. The same phenomenon has been described in previous reports. The initial modulus reduction is useful for improving the compliance of the vascular graft. Furthermore, it is notable that the tensile strengths (3.4–7.4 MPa (dry) and 2.3–6.2 MPa (wet)) and the strains (107–227% (dry), 117–180% (wet)) of the resulting scaffolds were comparable with those of native coronary arteries, which have a tensile strength of 1.4–11.1 MPa and a strain of 45–99%. The similarity in mechanical properties implies the DPA-loaded BPU scaffolds may mechanically match native arteries, which is important for the vascular graft patency.

Drug release kinetic

The DPA-loaded BPU scaffolds showed sustained drug release over a long time (91 days), as observed in in vitro studies. DPA is a small molecular and a highly hydrophobic drug. The release kinetics of the DPA-loaded BPU scaffolds was similar to those of paclitaxel-loaded polycaprolactone films and DPA loaded poly(lactide-co-glycolide) microspheres. The faster release during the first 3 days might be attributed to the low glass transition temperature (<−50 °C) from PCL segments in the BPU. The low burst release and the long-term release may be attributed to the hydrogen bonding between DPA and BPU, and the interaction between the hydrophobic DPA and the hydrophobic segment of BPU. The same phenomenon was found from a long-term

release of RheoSwitch Ligand 1 molecule (RSL1) loaded in a biodegradable polyurethane scaffold, where the hydrophobic RSL1 interacts with the polyurethane.

Human blood assessment

Compared to the BPU alone, the DPA-loaded BPU scaffolds had improved non-thrombogenicity (Figs. 2.5,2.6). The non-thrombogenicity is dependent on the DPA dose according to a previous report . In this study, the dose dependence was not distinct in non-thrombogenicity, whereas it was shown in HASMC proliferation inhibition. It may result from the different DPA dosages required for antithrombosis and SMC proliferation inhibition. The BPU scaffolds with higher DPA loading had better biofunction, and are capable of being implanted directly as a vascular graft with good patency.

In vitro cell studies

DPA was locally delivered into a rabbit model with carotid or femoral artery injury, and exhibited a dose-dependent inhibition of SMC proliferation. SMC proliferation inhibition was clearly found for BPU+5% DPA and BPU+10% DPA scaffolds, which loaded larger amounts of DPA.

The above results indicate that the released DPA from the scaffolds maintained its bioactivity after processing. It is notable that the DPA-loaded BPU scaffolds improved HAEC growth compared to the BPU alone . This implies that an EC layer would form quickly in vivo on DPA-loaded BPU scaffolds, which is important for biodegradable SDVG patency. It is controversial whether DPA promotes EC growth according to previous reports. For example, Liem et al. reported that 5 μM DPA inhibited proliferation of human ECs isolated from human umbilical cord. However, more reports have shown that DPA has a positive effect on vascular endothelial cell growth. Aldenhoff et al. concluded that

the DPA coating on a vascular graft as a bypass improved EC monolayer accommodation and thus showed increased patency in a sheep carotid artery model. Begandt et al. reported that DPA increased gap junction coupling of bovine aortic ECs, which resulted in better blood flow and increased vascular motility [49,50]. Guo et al. found that DPA reduced brain EC death after injury from oxygen–glucose deprivation by reperfusion. On the basis of the above reports, it is convincing that DPA would promote vascular endothelial cell growth, which is consistent with our observation in this work. On the other hand, spherical HAECs were seen on the scaffolds, especially on the BPU+10% DPA surface at day 7. This implies that the polyurethane surface might not strongly support the spread and growth of EC, which may be attributed to the hydrophobic surface and the absence of bioactive sites on the synthetic polyurethane. For example, bioactive modification, such as surface Arg–Gly–Asp–Ser (RGD) grafting on the polyurethane surface, was shown to be necessary to improve EC morphology and growth.

Limitations

Some limitations exist in this work. First, biomechanical testing of the vascular grafts, such as compliance and burst pressure, was not included. We will further evaluate the biomechanics of the vascular grafts prior to in vivo implantation in the future. Second, the HAEC accommodation is not ideal. Although DPA involvement improved the EC growth on the DPA-loaded BPU scaffold surfaces compared to the BPU surface, surface modification or conjugation of the polyurethane grafts with bioactive molecules needs to be further considered. Third, only in vitro evaluation was executed in this study. In vivo implantation will be performed in the future, which is a more effective way to assess the feasibility and biofunctions of the DPA released from SDVGs.

2.5 Summary

A biodegradable elastic nanofibrous scaffold with drug release was fabricated from a blend of a biodegradable polyurethane urea and a drug dipyridamole using co-electrospinning. The scaffold had tensile strength and strain comparable with human artery. The scaffold exhibited a long term drug release without obvious burst release till to 91 days. Compared to polymer alone, all scaffolds with drug release exhibited good blood compatibility with extended blood clot time, low hemolysis and human blood platelet deposition, especially for the scaffold with 10% drug loading. The scaffold at higher drug loaded content could improve human aortic endothelial cell proliferation and inhibit human smooth muscle cell growth. The dipyridamole drug release offered multiple biofunctions to the biodegradable nanofiborous elastic scaffold, which shows a promise to be applied for biodegradable small diameter vascular grafts and other blood-contact implants.

Chapter 3

Development of ECM-coated biodegradable nanoparticles to maximize lung cell uptake

3.1 Introduction

Lung diseases including chronic obstructive pulmonary disease, asthma, infections, as well as acute and chronic lung injury leading to fibrosis, constitute the third leading cause of death world-wide [28,76]. Inhalational drug delivery is a well-established route for targeted delivery of therapeutic agents (small molecules, proteins and DNA) to the distal lung, and is commonly employed in clinical as well as experimental settings [30,77]. Inhalational delivery takes advantage of the vast alveolar epithelial surface area to allow noninvasive delivery and rapid absorption of a large quantity of drug. Drug particles less than 5μm in diameter have a high probability of deposition in the lung while particles less than 2μm in diameter tend to concentrate in the alveoli. Nanoparticles have been used as carrier to deliver therapeutic reagents to the lung. Nanoparticles have the potential to target specific lung cells in the treatment of respiratory disease [77]. Incorporating drugs into nanoparticles provides additional benefits of increased drug concentration and sustained drug release, reducing the overall treatment dose and frequency, thereby decreasing local as well as systemic side effects [30].

On the other hand, maximizing the deposition of therapeutic agents at the alveolar air-tissue interface and the uptake by alveolar epithelial cells remain challenging owing to the cyclic nature of ventilation that reduces the time for particle deposition, the efficient airway muco-ciliary clearance system and the alveolar fluid lining layer that carry the delivered particles away from the epithelial cell surface, and the abundance of alveolar macrophages that detect and phagocytose particles especially those greater

than about 200nm in diameter. It has been estimated that only about 20-30% of an inhaled bolus actually reaches the lung and are take up by lung cells. Thus, there continues to be a need for novel carrier technology for improved drug delivery to and cellular uptake by the lungs.

To overcome the limitations of inhalational drug delivery via nanoparticles, various strategies, including surface modification, have been proposed to improve alveolar retention of nanoparticles. For instance, surface modification of calcitonin peptide-loaded PLGA nanoparticles with chitosan, a mucoadhesive material, demonstrates the prolonged effects of the peptide elcatonin compared to that of unmodified nanoparticles [31-32]. In addition, surface functionalization of anti-tuberculous antibiotics-loaded PLGA nanoparticles loaded with either chitosan or wheat germ agglutinin (WGA), a lectin with bioadhesive properties, provides significantly more sustained drug levels and reduces tubercle bacilli in the lungs of animals treated with these nanoparticles compared to those treated with non-conjugated nanoparticles [78-80]. Incorporation of nanoparticles with phospholipids and/or lung surfactants enhances pulmonary retention and reduces phagocytic uptake of nanoparticles, perhaps due to prevention of opsonic protein adsorption [33,35,81]. These observations indicate that surface modifications to enhance retention of drug-laden nanoparticle in the lung might be a useful strategy for improving pulmonary therapeutics.

Extracellular matrix (ECM), which consists of collagen, elastin, laminin, and proteoglycans, plays an important role in supporting diverse cell functions such as adhesion, viability and growth, has been widely used in the development of engineered tissues [82-83]. Over the last decade, ECM has been used to create biological scaffolds as replacement for organs/tissues such as heart valves [84-86], liver [87], kidney [88], and others [89-91]. Several studies have shown that incorporation of ECM or its

constitutive proteins and peptides provides adhesive cues and/or integrin-binding sites for cell adhesion to the synthetic polymers [92-95]. Little is known about the role of ECM in pulmonary therapeutics, and no study has examined the use of ECM in nanoparticle-facilitated drug delivery to the lung. Here we developed a novel formulation of biodegradable PLGA nanoparticles coated with lung-derived ECM by adsorption. We hypothesized that ECM coating improves adhesion interactions between nanoparticles and lung epithelial cells, thereby enhancing nanoparticle uptake and retention by lung cells.

3.2 Experiment section

3.2.1 Materials used

Poly (lactic-co-glycolic acid) (PLGA, 50:50) was purchased from the Lakeshore Biomaterials (Birmingham, AL). Sodium dodecyl sulfate (SDS), dichloromethane, 6-coumarin, and polyvinyl alcohol (PVA, MW 31,000-50,000 and 87-89 % hydrolyzed) were purchased from Sigma Aldrich (St. Louis, MO). Albumin from bovine serum (BSA) and Texas Red® conjugated BSA were purchased from Life technology (Carlsbad, CA). Type I alveolar epithelial cells (AEC1s) were purchased from Applied Biological Materials Inc. (Richmond, BC, Canada). All other chemicals were purchased from Sigma.

3.2.2 Preparation of porcine lung ECM solution

The porcine lung ECM solution was obtained by deceullarization and pepsin digestion as previously described [96]. Briefly, the lungs were harvested from adult pigs (weighing 80-100 kg) from a local slaughterhouse, cut into slices (1 mm in thickness) and rinsed using deionized (DI) water. Then the lung slices were processed by decellularization in 1% (w/v) SDS solution under stirring for 3-4 days, until the lung matrix

turned white. The SDS solution was refreshed every day. The decellularized matrix was rinsed using large amount of DI water overnight to remove SDS residual, and then freeze-dried for 3 day. The dry decellularized lung matrix further was solubilized at an ECM concentration of 15 mg/mL in 1mg/mL pepsin/0.01 M HCl solution. After 3 days, the decellularized lung matrix was solubilized without any visible particles. The solution was neutralized using 0.1 M NaOH and 10X PBS, and diluted to desirable ECM concentrations using 1X PBS for nanoparticle coating.

3.2.3 Fabrication of polymeric PLGA nanoparticles

PLGA nanoparticles (NPs) were fabricated using a modified double emulsion technique as previously described [97]. Briefly, 400 µL of 0.1% w/v Texas-Red BSA solution was added drop wise into 3 mL of 3.33% w/v PLGA solution that was dissolved in dichloromethane and then sonicated at 20W for 1 min. This first emulsion solution was then added drop wise to 12 mL of 5% PVA solution and sonicated at 40W for 3 min. This double emulsion solution was de-solvated overnight with stirring at room temperature. PLGA NPs were washed and collected using ultracentrifugation at 15,000 rpm for 30 minutes and lyophilization. The supernatant were collected to determine the loading efficiency of Texas-Red BSA. For cellular uptake and cell compatibility assessments, 6-coumarin loaded and unloaded PLGA NPs were fabricated using double-emulsion techniques as previously described [98].

3.2.4 PLGA NPs coated with porcine ECM by adsorption technique

PLGA NPs coated with porcine ECM were fabricated using modified adsorption technique [99]. Briefly, 10 mg NPs were suspended in 10 ml DI water and then mixed with 40 ml of porcine ECM solution at predetermined concentrations. The mixed solution

was rotated on a rotator for 24 h and then the nanoparticles were collected by ultracentrifugation at 15,000 rpm for 30 min. The collected NPs were freeze-dried for further use. As a positive control, PLGA NPs coated with rat tail collagen type I was fabricated by immersing uncoated PLGA NPs in a 0.01% w/v of collagen solution in 0.1 M acetic acid.

3.2.5 Optimization coating technique

PLGA NPs coated with porcine lung ECM were fabrication via absorption and layer by layer technique. The optimization of coating was determined by size measurement using DLS (according to nanoparticle characterization section) and cellular uptake study using bicinchoninic acid assay and coumarin-6 fluorescence readings (according to in vitro cellular uptake section).

3.2.6 Nanoparticle characterization

Particle size, polydispersity and zeta potential were measured using dynamic light scattering (DLS; ZetaPALS DLS detector, Brookhaven Instruments, Holtsville, NY). Nanoparticle solution were prepared at 1 mg/ml concentration, and added into the transparent cuvette with the fixed amount of de-ionized water for testing. The morphology of the nanoparticles was observed under a transmission electron microscope (TEM; Hitachi H-9500 High resolution Transmission Electron Microscope). Nanoparticle solution was dropped on an oxygen plasma treated and Formvar-coated 200-mesh copper grid (Electron Microscopy Sciences, Hartfield, PA). The water was removed using a filter paper and then 10 µL of 0.5% of vinyl acetate solution was dropped on the grid at room temperature. The sample was dried in the air overnight for imaging. In vitro stability of nanoparticles was evaluated using dynamic light scattering (DLS) in term of particle size

with time. Nanoparticle solutions at 1 mg/ml were prepared using PBS or cell culture medium with 10% fetal bovine serum (FBS; Atlanta Biological, Lawerenceville, GA), and were added into transparent cuvette. The cuvette was incubated at 37 °C for 2 d, and then the particle size was measured every 12 h using DLS instrument. Four replicates were used for analysis.

3.2.7 In vitro protein release kinetic profile

The stock solution of 1 mg/ml Texas-Red BSA-loaded PLGA NPs was added into a dialysis tubing (100 kDa molecular weight cut-off, Spectrum Laboratories Inc., Rancho Dominguez, CA), and then placed into PBS solution with pH 7.4 at 37^{o}C for 28 days. At pre-determined time points, 1 mL of dialysate was collected and kept in microcentrifuge tubes at -20^{o}C for future analysis, and 1 mL fresh PBS solution was replenished. The measurement of fluorescent intensity of Texas-Red BSA was performed on an ultraviolet-spectrophotometer (Infinite M-200, Tecan) at 480 nm (excitation) and 615 nm (emission). A Texas-Red BSA standard curve was recorded using series of BSA solutions with known concentrations to determine the concentration of released Texas-Red BSA. Four replicates were used.

3.2.8 In vitro human blood assessment

The protocol of human whole blood collection was approved by the Institutional Review Board (IRB) of the University of Texas at Arlington. Human whole blood was drawn into anti-coagulant tubes, which contain trisodium citrate, citric acid and dextrose. Nanoparticle solutions were prepared in 0.9% saline and then added into 1.5 mL microcentrifuge tubes. To prepare the human blood clotting solution, 0.85 mL of calcium chloride solution (0.1M) was added into 8.5 mL anti-coagulated blood, and then 50 µL of

blood were added into the tube containing nanoparticle solution. Blood solutions served as a control. After a pre-determined time point (10, 20, 30, and 60 minutes), 1.5 mL distilled water were added, and incubated at room temperature for 5 min to terminate the reaction. Then, 200 µL of the lysate were collected from each samples and added into 96-well plates. To determine the clotting cascade, the lysate were measured the absorbance at 540 nm using an ultraviolet-spectrometer (Infinite M-200, Tecan) [72]. Eight replicates were used for analysis.

Nanoparticle solutions at various concentrations were prepared in 0.9% saline. To prepare a negative control and a positive control, 200 µL of anti-coagulated blood were diluted in 10 ml 0.9% saline solution and 10 mL DI water, respectively. 10 µL of nanoparticle solution was added into a microcentrifuge tube and then 200 µL of blood solution were added. Samples were placed in an orbital shaker and incubated at 37 ^{o}C for 2 h. The samples were then centrifuged at 1000 g for 10 min to obtain the supernatant. The supernatant was transferred into a 96-well plate and the absorbance at 545 nm was recorded under an ultraviolet-spectrometer [73]. Eight replicates were used for analysis.

3.2.9 In vitro cytocompatibility

Human alveolar type I epithelial cells (AEC1s) were pre-seeded in collagen I cellware 96 well-plates (Corning, NY) at a density of 5000 cells per well and incubated at 37 °C and 5% CO2 for 24 h in Prigrow III medium with 10% fetal bovine serum (FBS) and 1% penicillin/streptomycin. The medium was then replaced with nanoparticle suspensions in medium at various concentrations (n = 4). After 24h incubation, the medium was removed and the samples were washed using PBS. The samples were treated with 3-(4,5-dimethylthiazol-2-yl)-5-(3-carboxymethoxyphenyl)-2-(4-sulfophenyl)-

2H-tetrazolium (MTS) reagent (CellTiter 96®AQueous One Solution Cell Proliferation Assay, Promega, Madison, WI) and incubated for 4 h following the manufacturer's instructions. Absorbance was detected using an ultraviolet-spectrometer (Infinite M200, Tecan) at 490 nm to determine cell viability.

3.2.10 In vitro cellular uptake

The 6-coumarin loaded-nanoparticle suspensions in medium were added into a AEC1s pre-seeded plate (5000 cells per well). After 2h incubation, the medium was removed and the samples were washed using PBS solution. The cells were lysed with 250 µL of 1% Triton X-100 for 30 min at 37 ^{o}C. Fluorescence intensity was then measured using a spectrophotometer to determine the 6-coumarin loaded nanoparticles taken up by the cells. These measurements were analyzed against an NP standard. The cell lysate sample is quantified for the total cell protein associated with the cell number using Pierce BCA protein assay for normalization with the particle uptake (Fisher Scientific, Hampton, NH) following manufacture's protocol. Confocal microscope was used to observe nanoparticle uptake inside the cells.

3.2.11 Inhalational delivery and examination of lung tissue in a rat model

The Institutional Animal Care and Use Committee of the University of Texas Southwestern Medical Center approved all procedures. Adult Sprague-Dawley rats (300-400 grams body weight) were anesthetized with an intraperitoneal injection of ketamine (50 mg/kg) and xylazine (5 mg/kg) and suspended by their front teeth on an angled fiberglass stand. The tongue was lifted with forceps and the trachea visualized using an otoscope. A 14 gauge cannula was inserted into the trachea using a guide wire. Nanoparticles were synthesized as described above, loaded with plasmid DNA vector

encoding hEPOR and co-expressing GFP. Each nanoparticle preparation (1mg) was suspended in 0.3 ml of sterile saline, sonicated (Model 300VT ultrasonic homogenizer, Biologics Inc., Manassas, VA), aerosolized using a pediatric mesh nebulizer (Aeroneb™, 4-6μm droplets) and delivered over 3 min into the lungs via a tracheal cannula. Control rats received PLGA nanoparticles loaded with plasmid vector in the same manner. Following intubation the rats were observed to ensure complete recovery from anesthesia. At 4, 8, 14, 21, and 28 days post-treatment, rats were scarified by an overdose of Euthasol™ (pentobarbital 86 mg/kg and phenytoin 11 mg/kg by intraperitoneal injection). The lungs were inflated in situ via tracheal instillation of 4% paraformaldehyde at 25 cmH2O of airway pressure and removed intact. The fixed lobes were serially sliced at 3 mm intervals and the slice faces imaged by a biofluorescence imager (IVIS Spectrum, Caliper Life Sciences, Waltham, MA). Tissue blocks were embedded in paraffin, and histological sections (4μm thickness) were examined under a fluorescent microscope (Axioscope, Carl Zeiss Microscopy, LLC, Thornwood, NY).

3.2.12 Statistical analysis

All data are mean ± standard deviation (SD). Statistical analysis was performed with Statview software using one-way ANOVA with post hoc Fisher's Protected Least Significant Difference test. $P < 0.05$ was considered as significant difference.

3.3 Results

3.3.1 Decellularized lung ECM and characterization

Fresh lungs were isolated from adult pigs and processed into an ECM solution through decellularization and enzymatic digestion using sodium dodecyl sulfate (SDS) (Figure 3.1) to prevent immune response, and verified by DNA residue quantification.

After decellulariztion, 49±4 ng/mg dry weight of residual DNA was detected, which is much lower than that of native lung tissue (1113±102 ng/mg dry weight). The decellularized ECM contains two major components, collagen (77±21%) and glycosamingoglycan (GAG, 2.2±1.2 µg/mg dry weight), along with a mixture of proteins, peptides and growth factors. The collagen content is higher (11±2%), while the GAG content is lower than that in native tissue (6 .0±1.9 ng/mg dry weight). After enzymatic digestion, a flowable ECM solution was obtained (Figure 3.1).

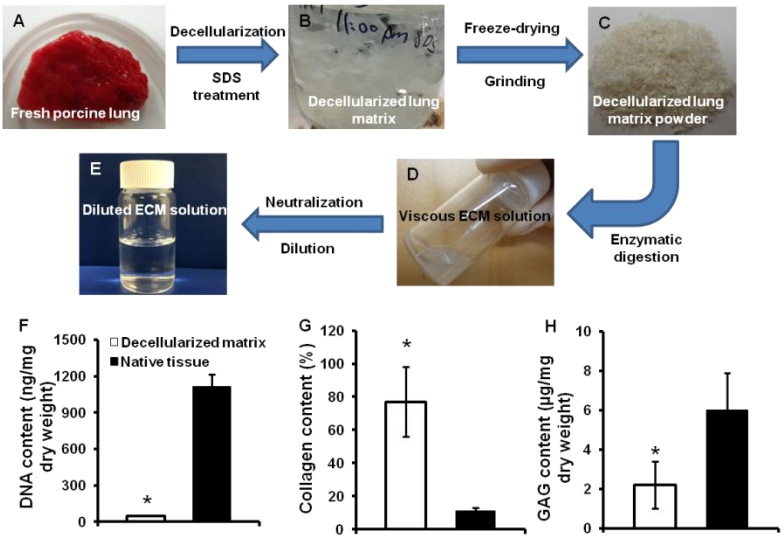

Figure 3.1: Decellularized lung ECM process and characterization. **(A)** Porcine lung was cut into small pieces (1mm thickness), then treated with 1%SDS solution **(B)** and followed by freeze dry **(C)**. The freeze dried decellularized powder was digested using pepsin solution **(D)** and followed by neutralization and dilution **(E)**. Characterization of lung ECM was quantified in term of DNA content (ng/mg dry weight) **(F)**, Collagen content (%) **(G)** and GAG content (µg/mg dry weight) **(H)**.

3.3.2 Optimization of coating technique base on size and cellular uptake studies

We optimized the coating technique base on the particle size, cellular uptake, ECM concentration and stability studies. We observed that increasing the ECM concentration revealed the larger diameter of NPs in both case of using absorption and layer by layer technique (Table 3.1). The cellular uptake of ECM-coated NPs showed the greater uptake compare to uncoated NPs. The cellular nanoparticle uptake reaches the maximum at the ECM concentration of 200 µg/ml (Figure 3.2). The stability study demonstrated the stability of 100 µg/ml concentration of ECM-coated NPs upto 48 h. However, 200 µg/ml concentration of ECM-coated NPs exhibit the aggregation of NPs after the reaction for 24-48h. Base on these observations, ECM concentration at 100µg/ml was choosed to use in this study.

Table 3.1: Size optimization of particles coated by adsorption and Layer-by-layer technique (LBL) using DLS measurement (mean ±SD , *n*=4).

Samples	Size (nm) Adsorption	Size (nm) LBL coasting
Coumarin-6 loaded PLGA NPs	197 ± 41	197 ± 41
Lung ECM-coated PLGA NPs		
100 ug/ml	242 ± 97	399 ± 323
200 ug/ml	226 ± 66	691 ± 366
300 ug/ml	409 ± 209	385 ± 198
500 ug/ml	301 ± 154	368 ± 191

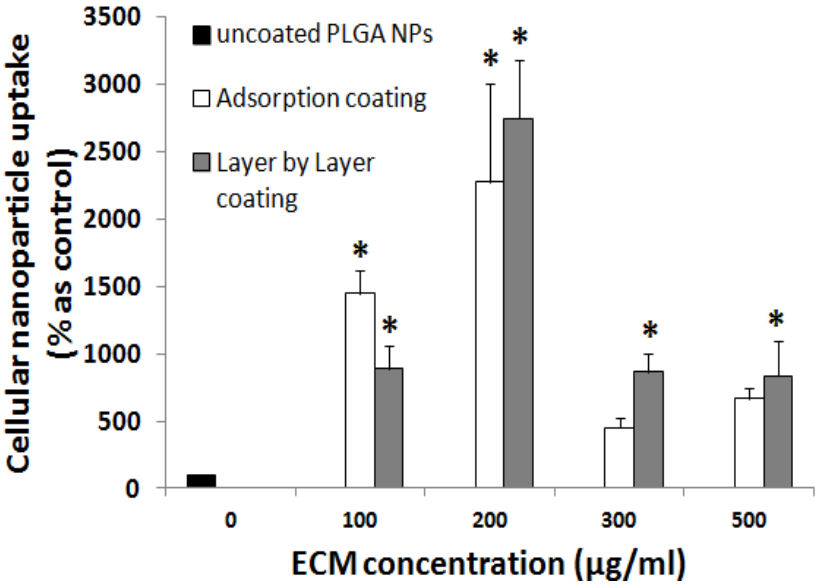

Figure 3.2: Optimization of coating technique (adsorption and LBL technique) based on cellular uptake of the NPs coated using difference ECM concentrations by AEC1s. Cellular uptake was measured using bicinchoninic acid assay and coumarin-6 fluorescence readings (n=4, $^{*}p < 0.05$ w.r.t. uncoated PLGA NPs).

3.3.3 Nanoparticle characterization

We coated NPs with a low concentration of ECM (100 µg/mL, Shown in Figure 3.3) to minimize the change in particle diameter, which might alter cellular uptake characteristics. No significant difference in particle diameter and surface charge was seen between uncoated (197 ± 41 nm) and ECM coated NPs (242 ± 97 nm) at ECM solution concentration of 100 µg/mL (Figure 3.3). TEM images demonstrated the uncoated NPs and ECM coated NPs (Figure 3.3B-C) had spherical shapes with similar diameter of around 100 nm. Stability study of uncoated and ECM-coated NPs was executed to detect the changes in particle sizes in different aqueous solutions at 37°C

including cell culture medium and PBS. Uncoated and ECM-coated NPs showed the good stability of NPs in PBS and cell culture medium referred to the NPs size measured by DLS measurement (Figure 3.3D-E). The particle size of ECM-coated NPs when tested in cell culture medium slightly increased in the first 12 hours and the size of ECM-coated NPs was close to the original size of NPs until 48 hours. The ECM-coated NPs remained stable in PBS solution up to 48 hours, so the ECM-coated NPs was considered as non-aggregated NPs with good stability (Figure 3.3D-E).

A

Coumarin-6 loaded into PLGA NPs	Size (nm)	Polydispersity	Zeta potential (mV)
Uncoated	197 ± 41	0.01± 0.03	-14.96 ± 1.74
ECM Coated (100 µg/ml)	242 ± 97	0.19 ± 0.04	-18.64 ± 0.98

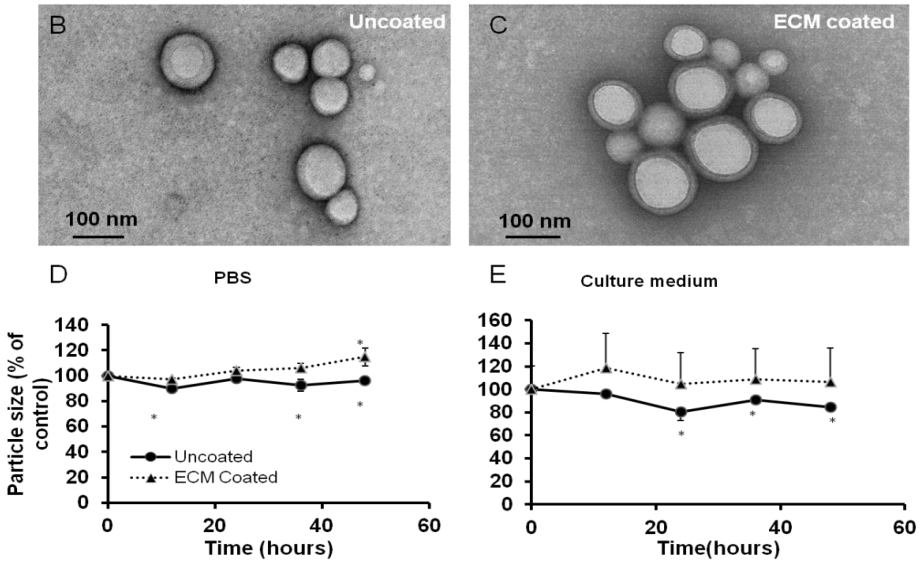

Figure 3.3: Uncoated and ECM-coated nanoparticle characterization. **(A)** Particle size, polydispersity and zeta potential were measured under DLS. TEM morphologies of uncoated **(B)** and ECM-coated **(C)** NPs reveal the spherical morphology. The stability study of uncoated and ECM-coated NPs was perform in PBS **(D)** and cell culture medium **(E)** at 37^{o}C upto 48h.

3.3.4 In vitro protein release kinetic profile

The ECM coating extended the payload release profile of Texas-Red bovine serum albumin (TR-BSA) (Figure 3.4). ECM-coated and uncoated NPs exhibited short-term burst release at day 1 followed by slower sustained release over 28 days. However, ECM coating reduced burst release from ~30% to ~ 20%, and markedly slowed sustained TR-BSA release compared to uncoated NPs. At day 28, 55% TR-BSA was released for the uncoated NPs, while 40% TR-BSA was release for the ECM coated NPs. The drug release mechanisms of uncoated PLGA NPs were accomplished by degradation followed by the diffusion. In ECM-coated NPs, the lower burst release displayed in the first 2 days might be the interaction/diffusion blocking of the ECM composition. However, the sustained release still remains up to 28 days.

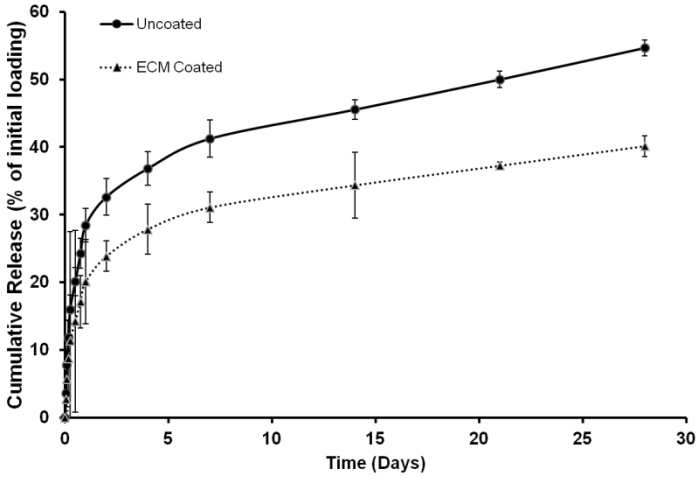

Figure 3.4: Bi-phasic Texas-Red BSA release profile of uncoated and ECM-coated NPs consisting of a burst release for the first day followed by sustained release for 4 weeks. ECM-coated NPs showed the initial burst release of 20% loaded drug within 24h.

3.3.5 Hemocompatibility of NPs

The ECM-coated PLGA NPs showed blood compatibility similar to that of uncoated PLGA NPs, verified by the blood clot and hemolysis tests (Figure 3.4). The blood alone showed an obvious clot at 30 min (Figure 3.5A). Similar to the blood alone, the obvious clots were observed at 30 min for both the uncoated PLGA NPs and ECM coated PLGA NPs (Figure 3.5B-C). The absorbance of the lysate for blood alone, uncoated and ECM coated NPs showed the same trend (Figure 3.5D). The hemolysis rates of uncoated and ECM coated NPs were very low (< 2%) without significant difference at different NP concentrations (Figure 3.5E). For all NP concentrations (0-1000 µgmg/ml), no significant difference exists ($p>0.05$).

Blood coagulation process was tested using hemoglobin solution under blood clotting measurement. The absorbance values of hemoglobin solution indicated the degree of blood clot. A High absorbance value represents high hemoglobin in the solution and less blood clotted formation and vice versa. We observed the decreasing trend of the absorbance value in control, uncoated and ECM-coated NPs as time progressed. These results showed that control, uncoated and ECM-coated NPs group exhibited similar blood clotting formation, suggesting ECM-coated NPs did not alter the blood clotting cascade based on absorbance values and the clotting images (Figure 3.5).

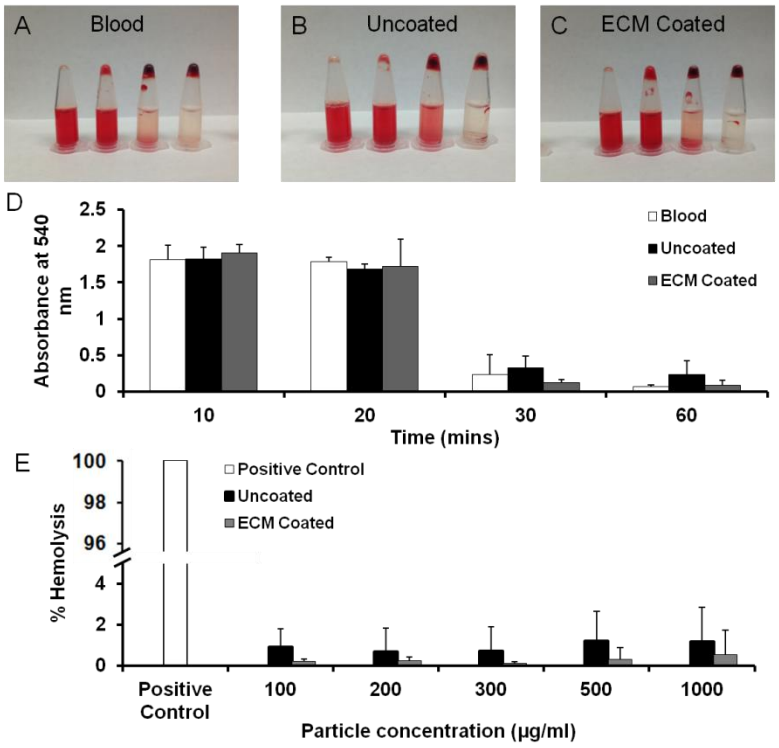

Figure 3.5: Digital images to show human blood clot formation with time of **(A)** human blood, **(B)** uncoated NPs in the human blood and **(C)** ECM-coated in the human blood. **(D)** The absorbance at 540 nm of the lysate of human blood contacted with the uncoated and ECM-coated NPs. **(E)** Human blood hemolysis percentages of the NPs.

3.3.6 In vitro cytotoxicity

The impact of increasing concentration of uncoated and ECM-coated NPs on Human alveolar Type I epithelial cells following 24 h incubation was studied and shown in Figure 3.5. Pre-seeded cell with expose to any NPs was chosen as a control. It has been shown that the alveolar Type I cells incubated with uncoated and ECM-coated NPs revealed over 90% viability up to the NP concentration from 100-1000 µg/ml compared to the control cells (Figure 3.6). This indicates uncoated and ECM-cotaed NPs are

cytocompatible and should not have any down side effects to the cells following administration *in vivo*.

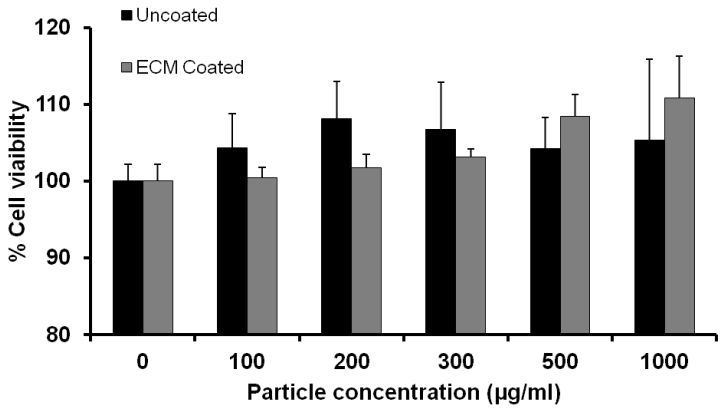

Figure 3.6: *In vitro* cell studies of uncoated and ECM-coated NPs at 37^{o}C for 24 h; AEC1s viability studies using an MTS assay indicated that uncoated PLGA NPs and 100 µg/ml ECM coated PLGA NPs have good cytocompatibility up to a feeding concentration of 1000 µg/ml.

3.3.7 Cellular Uptake by Type I Lung Epithelial Cells

The cellular uptake of uncoated, collagen-coated and ECM-coated NPs by human alveolar Type I epithelial cells was studied for 2 h. It has been shown that the uptaken of ECM-coated PLGA NPs was 28-fold higher than uncoated PLGA NPs and 15-fold higher than collagen-coated NPs at 1000 µg/ml NP concentration. Moreover, at a feed of 500 µg/ml NP concentration, the uptake of ECM-coated NPs demonstrated 24-fold higher than uncoated and 13-fold higher than collagen-coated NPs. The collagen-coated NPs also exhibit 1.8- fold higher than uncoated NPs at 500 and 1000 µg/ml of NPs concentration (Figure 3.7A).

Confocal microscopy was performed to observer NPs uptake after incubation with Type I epithelial cells for 2 h followed by fixation reagent for 30 min (Figure 3.7B).. ECM-coated NPs shown the higher fluorescence intensity of 6-coumarin dye which were incorporated for imaging purpose, which indicated more ECM-coated NPs were uptaken by cells compared to the uncoated NPs. Furthermore, the NPs stayed in the cell plasma other than cell nuclei.

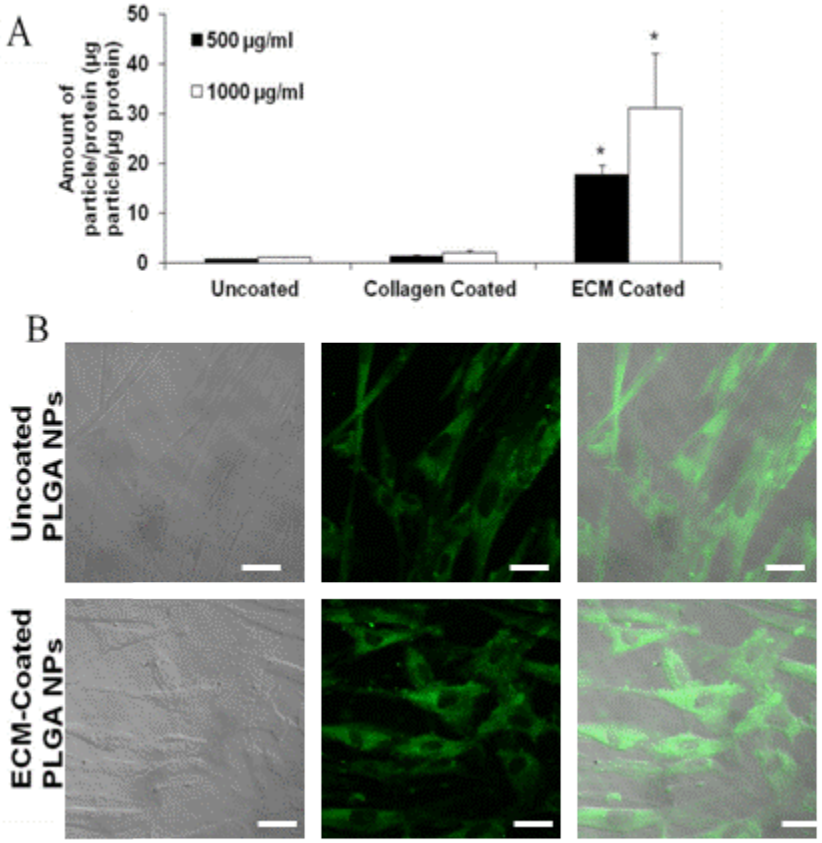

Figure 3.7: Cellular uptake of NPs coated with collagen and ECM by AEC1s was detected using bicinchoninic acid assay and coumarin-6 fluorescence **(A)**. Fluorescent images of uncoated and ECM-coated PLGA NPs uptaken by AEC1s show that ECM coating greatly enhanced cellular uptake of NPs **(B)**.

3.3.8 *In vivo* study

The tissue fluorescence images (Figure 3.8) showed that the GFP expression from uncoated PLGA NPs with hEPOR was found in airway at Day 8, with increased concentration in the lung tissue and finally penetrated deeper regions of the lungs parenchyma. For uncoated NP loaded with hEPOR, the GFP expression increased with the delivery time during a period of 21 days (Figure 3.8). For ECM-coated NPs, the GFP expression showed a maxmium value at day 14, and then decreased. The lower GFP expression at early stage of ECM-coated NPs was detected which corresponded with the drug release result. Overtime the ECM-coated NPs were found more in the airway and pleura region which indicated potential tendency NPs to diffuse out systemic circulation. High fluorescence radiants were detected at the airway and the pleura region which can be attributed to the blood flow causing shear stress/rate. Size of NPs could also be the factor that causes the particle accumulation in those regions. In terms of the *in vitro* drug release and tissue fluorescence, the blood flow might be the influential factor over NPs attachment on the surface of the lung.

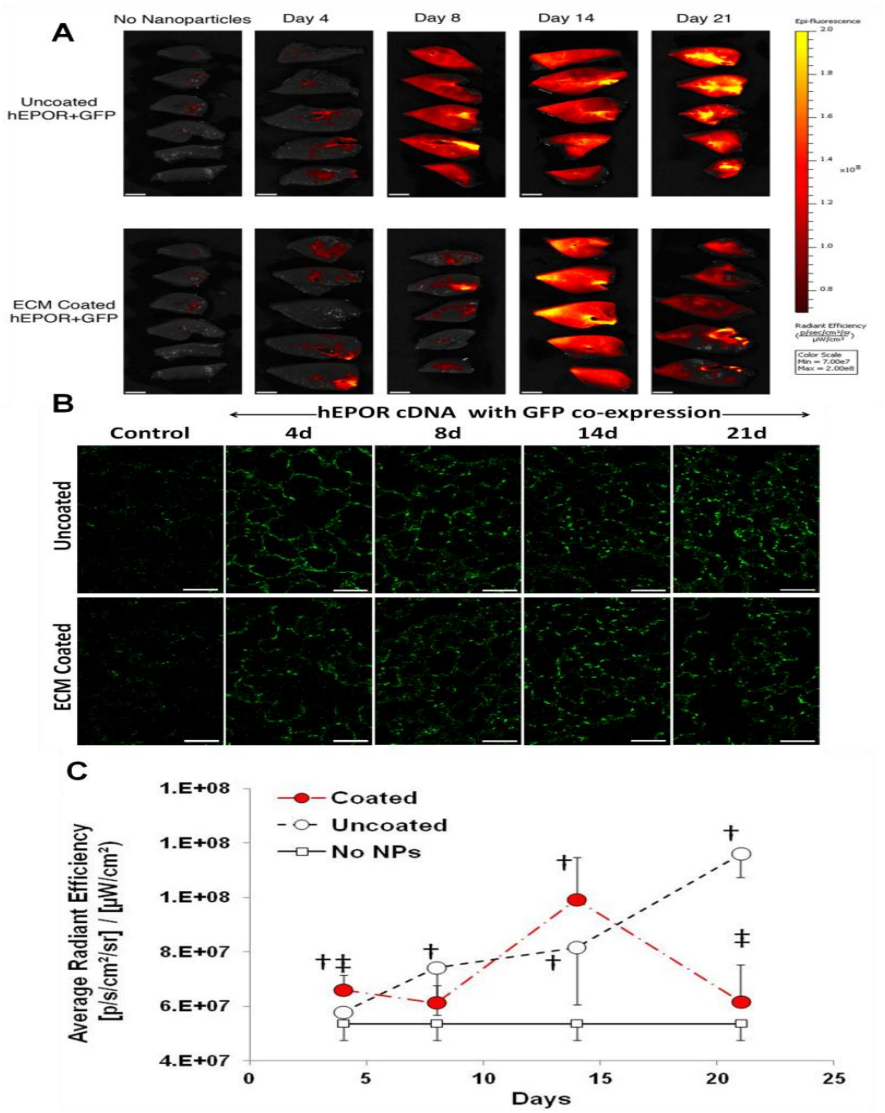

Figure 3.8: Inhalation delivery of GFP-tagged cDNA loaded uncoated or ECM-coated PLGA NPs to rats. GFP expression is shown in lungs fixed on different days following inhalation, examined by biofluorescence imager **(A)** and fluorescent microscopy **(B)**. GFP expression measured by the average radiant efficiency **(C)** progressively increases over 21 days in uncoated NPs. ECM-coated NPs demonstrate earlier peak of gene expression by day 14.

3.4 Discussion

Lung-derived ECM

The decellularization of the whole lung has been conducted, and the recellularized lung ECM scaffold supported the lung inhalation and gas exchange after implantation into a rat lung. The extracellular matrix of the lung has biomimetic structure and components with native tissue, which provide physical and chemical cues for lung cell growth and differentiation. The enzyme treatment can further cut down molecular weight of ECM to make it soluable. The ECM contains many biological components, such as collagen, elastin, GAG, and other unknown biological components. Some groups have detected over 30 proteins using a mass spectrometer. It has reported that the degradation products of the ECM has functions in cell recruiting, proliferation and migration. The decellularization and solublization process is an established technique, and has been popular for isolating tissue-derived ECM. The main challenge is to maximally preserver biological components, especially the water-soluble bioactive molecules while completely removing cellular components that might cause an immunogenic response. As the whole process is conducted in water, some water-soluble biomacromolecules, such as GAG, would be washed away. Because SDS is a strong positively charged detergent that accelerates the separation of some proteins from ECM as a result of conjugation. SDS residue is potentially toxic, thus the ECM was washed with a large amount of DI water. The decellularized product using SDS has been evaluated in vitro and in vivo, and no cytotoxicity or significant immune response was observed from previous reports. Meanwhile, other detergents such as Triton X100, and peracetic acid may be able to use for lung decellularization to preserve more bioactive molecules for this purpose.

ECM-coated NPs

Uncoated PLAG NPs was successfully fabricated using emulsion method. The nanoparticle size measured by dynamic light scattering and transmission electron microscopy were significant difference in terms of the hydrodynamic and actual diameter. Prabha et al. mentioned that dynamic light scattering gives the hydrodynamic diameter instead of the actual diameter. Therefore, we investigate the actual diameter using transmission microscopy which revealed around 100 nm. The hydrodynamic and actual diameter size of ECM-coated NPs were increased compared to uncoated NPs revealed the successfully protein adsorption on the surface of the NPs. Ehrenberg et al. reported that coating NPs with protein serum via adsorption slightly increased the size of the NPs around 15-25 nm and effected the surfaces charge of NPs. Similarly to our results, the size of ECM-coated NPs was larger than uncoated NPs in both hydrodynamic and actual diameter

Stability study of uncoated and ECM-coated NPs was carried to demonstrate the particle sizes stability in different aqueous solutions at 37°C such as cell culture medium and PBS. Uncoated NPs showed the stability of NPs in PBS and cell culture medium referred to the NPs size measured by DLS measurement upto 48 hrs which agreed to our previous studies. The particle size of ECM-coated NPs when tested in cell culture medium was slightly increased in the first 12h which might be caused by protein interaction with the NPs. Likewise, ECM-coated NPs remained the stable in PBS solution up to 48h , therefore, ECM-coated NPs was considered as non-aggregated NPs. Moreover, the washing step and centrifugation optimization maybe the key answers to deal with this issue.

To coat polymeric NPs with polymer or biomolecules, many techniques have been widely used such as adsorption and layer by layer. In this study, we coated PLGA

NPs with ECM solutions at various concentration using these two techniques. After optimization, we decide to select PLGA coated with ECM solution at 100 µg/ml to continue the studies base on particle size and cellular uptake behavior.

To characterize the uncoated and ECM coated PLGA NPs properties, dynamic light scattering, Zeta potential and transmission electron microscopy were used. The particles size of ECM coated PLGA NPs was slightly higher than uncoated PLGA NPs which verified the coating success. Moreover, zeta potential of ECM coated NPs was changes because of the surface charges alternation.

Blood compatibility and cell compatibility

Hemocompatibility studies of uncoated and ECM-coated NPs were conducted using hemolysis and blood clotting time. The effect of biomaterials on erythrocyte was tested and explained by hemolysis study. To investigate the damage of the biomaterial to erythrocytes, hemolysis study was performed. Autian has been mentioned that less than 5% of hemolysis rate of biomaterial were permitted. Base on our results, we claimed that ECM-coated NPs are non-hemolytic and comparable to uncoated PLGA NPs which has been shown great hemocompatibility.

Blood coagulation process was tested using hemoglobin solution under blood clotting measurement. The amount of blood coagulation can be determined by the absorbance values of hemoglobin solution indicating the degree of blood clot. Dey et al. mentioned that High absorbance value represents high hemoglobin in the solution and less blood clotted formation and vice versa. Base on our result, uncoated NPs revealed that good compatibility to the blood coagutaiton factor. ECM coated NPs exhibit similar behavior to uncoated NPs which indicating the good hemocompatibility.

In vitro cytocompatibility was conducted using MTS assay to determine the cell viability of our NPs system. Uncoated and ECM-coated NPs revealed the percentage of cell viability similar to control (TCPS) with AEC1s at 0-1,000 µg/ml NPs concentration which is correlated to the previous results of uncoated PLGA NPs cytocompatibility. Uncoated PLGA NPs has been investigated about cytotoxicity of the material to the many types of healthy cells and been proven that uncoated PLGA NPs are cytocompatible. Coating PLGA NPs with polymers or biomolecules can be affected the toxicity of the nanomaterial to the cells depends on the coating materials. In this case, ECM solution which comprise of many biomolecules, proteins and proteoclycans suppose to create non-toxicity to the cells which we can be observed by the higher percentages of cell viability of ECM-coated PLGA NPs. The composition of ECM should play a major role in facilitating of cell proliferation to explain the high percentage of cell viability.

Lung tissue has abundant vascular supply, and the NPs could penetrate the vascular wall and enter the circulation. PLGA is a popular FDA-approved biodegradable polymer. Both the polymer and its degradation products are biocompatible. We previously showed that PLGA NPs are biocompatible with type I alveolar epithelial cells. Decellularized ECM is highly cytocompatible according to previous reports. Thus, it is not surprising that the combination of PLGA and ECM also exhibits high cellular compatibility.

Drug release kinetic

In vitro protein release kinetic study of uncoated and ECM-coated NPs was carry out over 28 d. Uncoated NPs revealed the burst release within 2d and sustained release up to 28d in agreement with our previous study. The drug release of uncoated PLGA NPs majority released out from NPs by degradation mechanism followed by the diffusion mechanism. In ECM-coated NPs, the lower burst release displayed in the first 2d might

be the interaction/diffusion blocking of the ECM composition coating. Given that drug diffusion and carrier degradation are two major factors that determine drug release kinetics, these results indicate that the ECM coating layer acted as a barrier to retard BSA diffusion from the PLGA core. The phenomena have been reported in similar case which coated with PEG.This barrier can reduce the protein loss during the drug release mechanism transportation, and increase protein release amount at the target site.

In vitro cellular uptake

While cellular affinity peptides, such as RGD and TAT, have been shown to enhance nanoparticle uptake by cells, these are the first data to show that ECM coating also enhances nanoparticle uptake. As collagen is a major component in the ECM, we used pure type I collagen coating as a control, which did not significantly increase nanoparticle uptake, suggesting that other bioactive components in the ECM are responsible for facilitating nanoparticle uptake. Owing to the complex composition of the ECM solution, further studies will be needed to identify and isolate the factors and the mechanisms responsible for the enhancement in uptake.

The cellular uptakes of NPs were correlated to type of cells, time and dosage. In this study, the mammalian cell AEC1s was used to perform cellular uptake to our NPs with 2h incubation time. Dose-dependent of cellular uptake was observed when we increased the concentration of NPs. The cellular uptake of NPs also involve with the NPs size, surface charge and hydrophobicity by endocytosis mechanism. The higher cellular uptake correlated to smaller NPs size, negative charge and low hydrophobicity. Interestingly, ECM coated NPs revealed greater cellular uptake compared to uncoated NPs and collagen coated NPs at 500 and 1000 μg/ml of NPs concentration. This phenomenon can be explained by the cell adhesion of the NPs, the interaction between

NPs and cell membrane as well as the ECM properties. Sahoo et al. revealed the higher amount of PVA on the surface of NPs reduce the cellular uptake affinity. Therefore, ECM-coated NPs with suppose to have less PVA due to the coating process may be another factor the cellular uptake.

In vivo protein expression

The tissue fluorescence images suggests that the GFP expression from uncoated PLGA NPs was initially found in airway (d8), with increased concentration in the lung tissue and finally penetrated deeper regions of the lungs parenchyma. For ECM coated NPs, lower fluoresces was detected which correspond with drug release result. Overtime the ECM coated NPs were found more in the airway and pleura region which indicated potential tendency NPs to diffuse out systemic circulation. High fluorescence radiant were detected at the airway and the pleura region which can be attributed to the blood flow causing shear stress/rate. Size of NPs could also be the factor that cause the particle accumulates to those regions. From the in vitro drug release and tissue fluorescence, it is possible that blood flow might be the influential factor over NPs attachment on the surface of the lung which was not a parameter in the in vitro drug release study. It is likely that the ECM coating acts as an additional barrier with slower degradation kinetics than PLGA, thus retaining the cDNA released from PLGA degradation and delaying peak protein expression in tissue. The mechanism for the short duration of delayed peak protein expression is not clear. The accelerated decline in fluorescent protein expression between days 14 and 21 suggests that ECM may accelerate the peak of GFP expression degradation. ECM is a complex substance that is known to modulate cellular metabolism and immune response as well as facilitate tissue

protection and repair in vivo.Thus, ECM coating may also modulate the expression of the encapsulated gene or protein.

3.5 Summary

PLGA NPs coated with lung-specific ECM show delayed burst release followed by sustained release of the encapsulated agents, and exhibit excellent cytocompatibility and hemocompatibility. The ECM coating markedly enhances NP uptake by AEC1s, and accelerates the time to peak gene expression with similarly persistent downstream signal transduction compared to uncoated NPs. For pulmonary delivery, the uncoated NP formulation is suitable for progressive payload release and prolonged tissue expression, while the ECM-coated formulation is well suited for extremely rapid uptake, delayed core release and more precisely timed target gene expression.

Chapter 4

Conclusions and preliminary results of future works

4.1 Conclusions

To summarize the whole story of this dissertation, the nanostructured biomaterial has been successfully fabricated by electrospinning technique as a scaffold and double emulsion technique as a nanoparticle. The executed characterization, *in vitro* and *in vivo* biological studies further verified their properties and potential applications in clinic for human healthcare.

The first project is to synthesize a polyurethane nanofibrous scaffold incorporated with dipyridamole as a vascular conduit. Dipyridamole was sustained release from polyurethane scaffold for over 91 days, and this vascular graft has been shown the great mechanical properties to match the native arteries. Moreover, intimal hyperplasia challenge can be overcome by inhibiting proliferation of smooth muscle cells, promoting the endothelial cell formation and preventing thrombosis. The dipyridamole drug release offered multiple bio-functions to the biodegradable nanofibrous elastic conduit, which would find opportunities to be used for biodegradable small-diameter vascular grafts and other blood-contact devices.

The second project is to synthesize nanostructured biomaterial as a nanoparticle which has been coated with extracellular matrix. The purpose of this project is to minimize the dose of nanoparticle in the body and maximize the NP retention and uptake activities of the lung cells. PLGA NPs coated with lung-specific ECM showed lower burst release with good cyto-compatibility and hemo-compatibility. The ECM coating markedly enhances NP uptake by AEC1s, and accelerates the time to peak gene expression compared to uncoated NPs. For pulmonary delivery, the uncoated NP formulation is suitable for progressive payload release and prolonged tissue expression, while the

ECM-coated formulation is well suited for extremely rapid uptake, delayed core release and more precisely timed target gene expression. This ECM-coated nanoparticle drug delivery system would be promising to be applied for lung repair and regeneration, and for other disease treatment.

4.2 Future works

In terms of the student health condition, there are some studies, which have been suggested from the doctoral comprehensive exam's committee members, could not be done. Those include the scaffold shrinkage study in 3D dimension (Aim1), and nanoparticle localization inside the alveolar epithelial cells (Aim 2). Due to his health conditions, he completed the dissertation with major help from Drs. Yi Hong and Kytai T. Nguyen.

Base on the current results, the future work of the first project will focus on the *in vivo* study of the vascular conduit. In the current results, we performed *in vitro* experiments and have observed promising results in good blood compatibility with improved endothelial cell growth and reduced smooth muscle cell proliferation, which exhibit high promise to be tested in an animal model. In addition, further optimization, such as alternative drugs and polymer composition is necessary to achieve an ideal biodegradable conduit with good biofunctions and well mechanical match. Selecting a new powerful and practical drug with multiple functions is very important to improve this system as the DPA is not popular to be used in clinic right now.

The second project is to maximize the cellular retention and uptake activities of the nanoparticle and minimize the nanoparticle dose to reduce possible side effects. To investigate the nanoparticle location inside the cell, it could the great future work of this project which help us to understand the phenomenon of the greater cellular uptake of

ECM-coated nanoparticle. Furthermore, the ECM composition needs to be clearly analyzed to find the key elements in promoting cell uptake, which would be very useful for understanding associated mechanisms and future broad applications. Finally, more *in vivo* studies could be performed to verify the outcome and feasibility in lung repair and regeneration using various lung injure animal models.

Furthermore, the advanced nanostructured scaffolds need to be designed for various and broadened biomedical applications. On the basis of this consideration, we continue to design a new nanostrutured scaffolds with nanofibers and nanoparticles for potential wound healing use, which is a popular and hot area in biomaterial applications. Such hybrid scaffolds will combine advantages from both nanofibers and nanoparticles into one, which may be more appropriate to provide solutions to wound healing scaffolds with critic requirements in mechanics and biofunctions. The nanofibers can provide flexible, soft and robust mechanical supports, and nanoparticles can provide required biofunctions, such as anti-infection, by drug release. We have started this project, and summarized preliminary results as below.

4.3 Preliminary results of future works in nanoscaffolds for wound healing

4.3.1 Introduction

Over a million of patients were affected by chronic wound, and approximately 20 billion dollars annually were expensed [100]. Thus new strategies or alternative treatments are needed to combat this disease. Wound healing process has 5 phases to go through which include homeostasis, inflammation, migration, proliferation and remodeling [41]. Traditional wound dressing only prevents bacterial infection but does not provide an appropriate environment for a healing process [40]. Currently, wound dressing has been developed over a past decade to act as a barrier for secondary infection and

provide an excellent environment for regeneration [101]. To enhance the healing process, biological wound dressing has been fabricated such as hyaluronan-based scaffolds [102], collagen-based wound dressing [103], and chitosan-based scaffold [104]. It has been proved that the healing process were expedited after using biological wound dressing, however inappropriate mechanical properties, low biostability and immunes responses are the drawbacks [105]. To solve these problems, the wound dressing fabricated from synthetic polymers, including polyurethane [106], polylactic-glycolic acid [107], and polycaprolactone [108], is an alternative way to provide better mechanical properties compared to those of natural wound dressing.

Research efforts have shown that electrospun synthetic biodegradable polymer nanofibers is a great potential candidate for wound dressing due to large surface area, high porosity, rapid cell attachment/proliferation, and controllable drug release [109]. Moreover, ECM-like scaffold can be prepared via electrospinning to promote cell proliferation [110]. However, it still cannot meet the requirement of ideal wound dressing which comprised of various characteristics, such as physical properties, mechanical properties, anti-infection, physiological environment, and cell attachment and proliferation [111].

In this study, we focused on creating a hybrid nanostructured scaffold that could prevent bacterial infection, provide mechanical support, and supply physiological environment for cell proliferation. The polyurethane containing biodegradable nanoparticles loaded with antibiotics were electrospun into a nanofibrous scaffold for skin wound healing applications. The biodegradable polyurethane nanofibers provide the large surface area and mechanical support as a wound dressing, while antibiotic drug release can prevent infection. The scaffold was preliminary tested for bacteria inhibition properties. We also tried to incorporate antimicrobial peptides into biodegradable polymer

nanoparticles, and then combine the biodegradable nanoparticles with polyurethane fibers for synergistic anti-microbial effects.

4.3.2 Experiment section

4.3.2.1 Materials used

Polycaprolactone diol (PCL, Mn = 2,000), putrescine and hexamethylene diisocyanate (HDI;) dichloromethane, 6-coumarin, polyvinyl alcohol (PVA, MW 31,000-50,000 and 87-89 % hydrolyzed), and Vancomycin were purchased from Sigma Aldrich (St. Louis, MO). Anhydrous dimethyl sulfone (DMSO; Sigma), isopropanol (Sigma) and 1,1,1,3,3,3-hexafluoro-2-propanol (HFIP; Oakwood Products) were used as received. Poly (lactic-co-glycolic acid) (PLGA, 50:50) was purchased from the Lakeshore Biomaterials (Birmingham, AL). Vancomycin and Tigeclycline was purchased from Fisher Scientific. All other chemicals were purchased from Sigma.

4.3.2.2 Synthesis of PU

The biodegradable PU was synthesized using a modification of a protocol described previously [69]. Briefly, PCL was dissolved in DMSO in a three-necked flask with nitrogen protection, then HDI and three droplets of the catalyst $Sn(Oct)_2$ were added. After 3 h at 70 °C, the mixture was cooled down to room temperature. A putrescine/DMSO solution was then added to the flask with agitation. The molar ratio of PCL/HDI/putrescine was 1:2:1, and the final polymer concentration in the flask was around 4% (w/v). The flask was kept at 70 °C overnight, whereafter the polymer was precipitated in deionized water. The obtained polymer was rinsed three times in a large amount of water, then immersed in isopropanol to further remove unreacted monomers

and oligomers. Then the obtained PU was dried in a vacuum oven at 60 °C for 3 days. The yield was above 85%.

4.3.2.3 Fabrication of electrospun antibiotic drug-loaded nanofibrous scaffolds

PU and Vancomycin or Tigecycline were mixed and dissolved in HFIP at concentrations of 1% to PU. The PU concentration was 6% (w/v) in the solution. The mixed solution was loaded into a 10 ml syringe connected to a stainless steel capillary. The capillary was charged with a high voltage of 12 kV, and a conductive metal collector covered with an aluminum foil was charged at −10 kV. The distance between the capillary tip and the collector was 30 cm. The collector was rastered at a speed of 5 cm s^{-1} on both the x and y axes (Velmex Inc., USA). The mixed solution was electrospun vertically at a flow rate of 1 ml h^{-1}. After 4 h, the electrospun sheets were removed from the foil and dried overnight in a vacuum desiccator for further use.

4.3.2.4 Fabrication of polymeric PLGA nanoparticles

PLGA nanoparticles (NPs) were fabricated using a modified double emulsion technique as previously described [97]. Briefly, 200 µL of 0.1% w/v antimicrobial peptide solution or antibiotics was added drop wise into 3 mL of 3% w/v PLGA solution that was dissolved in dichloromethane and then sonicated at 20W for 1 min. This first emulsion solution was then added drop wise to 12 mL of 5% PVA solution and sonicated at 40W for 3 min. This double emulsion solution was de-solvated overnight with stirring at room temperature. PLGA NPs were washed and collected using ultracentrifugation at 15,000 rpm for 30 minutes and lyophilization.

4.3.2.5 Fabrication of electrospun nanoparticle-loaded nanofibrous scaffolds

PU and nanoparticle containing antimicrobial peptide were mixed and dissolved in HFIP at concentrations of 10-20% to BPU (w/w). The PU concentration was 6% (w/v) in the solution. The mixed solution was loaded into a 10 ml syringe connected to a stainless steel capillary. The capillary was charged with a high voltage of 12 kV, and a conductive metal collector covered with an aluminum foil was charged at −10 kV. The distance between the capillary tip and the collector was 30 cm. The collector was rastered at a speed of 5 cm s^{-1} on both the x and y axes (Velmex Inc., USA). The mixed solution was electrospun vertically at a flow rate of 1 ml h–1. After 4 h, the electrospun sheets were removed from the foil and dried overnight in a vacuum desiccator for further use.

4.3.2.6 Scaffold characterization

The electrospun nanofibrous sheets containing either antimicrobial peptide or antibiotic drug were sputter-coated with silver and their surface morphology was then observed using a scanning electron microscope (SEM; Hitachi, S-3000N). The fiber diameter was measured using software ImageJ (National Institutes of Health).

4.3.2.7 Antibacterial assessment

To observe the inhibition activity of nanofibrous composite sheets containing antibiotic drug and/or antimicrobial peptides, Gram-positive bacteria *S.Aureus* (ATCC) was used in this study. Briefly, *S.Aureus* was reconstituted in LB-medium following manufacturer's instruction, and then spread on to the LB agar-plate to obtain the single colony. Select 1 single colony to sub-culture in LB-medium for 4 hrs to obtain the bacteria concentration approximately 10^6 CFU ml^{-1}. Swabbing the bacteria solution on to the LB-

agar plate and place the samples on top of it, followed by incubation at 37^0C overnight. The next day, the bacteria inhibition zone were observed and measured by calibration ruler.

To observe the bacteria growth curve, samples were added into bacteria suspension and incubated at 37 °C. At predetermine time-point, the bacteria suspension was took out and read the absorbance at 600 nm. Averages of background samples (broth without bacteria) were subtracted from bacterial samples and plotted over a time course. Bacteria suspension cultured with antibiotic drug (ampicillin at 50mg/ml concentration) was used as a positive control. All operations were performed under aseptic conditions.

4.3.3 Preliminary Results and Discussion

4.3.3.1 Scaffold characterization

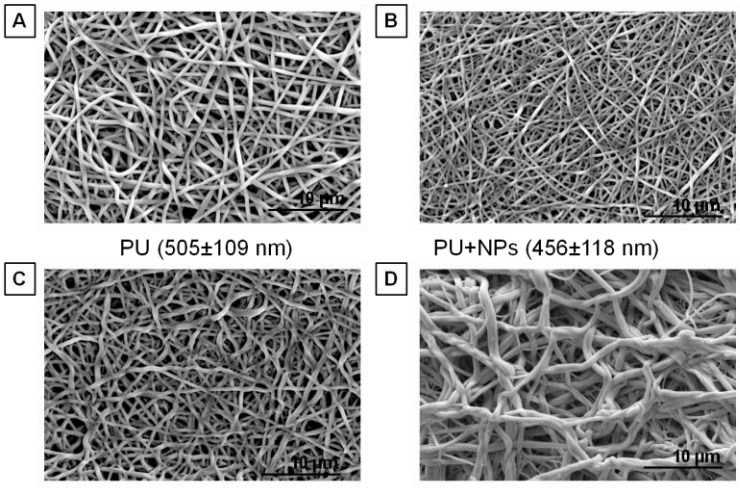

Figure 4.1: Micrographic fiber morphologies of **(A)** 6% PU, **(B)** 6% PU loaded with nanoparticle, **(C)** 6%PU loaded with antibiotic drug **(D)** 6% PU loaded with nanoparticle and antibiotic drug.

A nanofibrous scaffold was fabricated by electrospinning without beads in SEM images (Figure 4.1). The fiber diameters of the 6%PU, 6%PU loaded with nanoparticles, 6% PU loaded with antibiotic drug and 6% PU loaded with antibiotic drug and nanoparticles containing antimicrobial peptides are 505±109, 458±118 , 496±116, and 868±225 nm respectively.

4.3.3.2 Antibacterial assessment

Nanofibrous sheets containing NPs loaded with antimicrobial peptide or antibiotic drug such as tigecycline and vancomycin were used to performed inhibition zone study of *S.Aureus*. The concentration of S.Aureus was determined by OD_{600} and approximates the number of colony around 10^6 CFU ml^{-1}. The concentration of antibiotic drug was fixed as 1% w/v of polymer concentration base on minimal inhibitory concentration (MIC) of the drug. As shown in Figure 4.2, PU alone and PU loaded with nanoparticle did not show any zone of inhibition of *S.Aureus* after 24 hours of incubation. On the other hand, PU loaded with antibiotic drug revealed the inhibition zone of *S.Aureus*. To determine the inhibitory activity of the drug, Table 4.1 revealed the inhibition zone in term of radius (mm) of the samples. PU loaded with Vancomycin and Tigecycline exhibited the zone of inhibition around 8.09±0.41 mm and 19.36±0.76 mm, respectively.

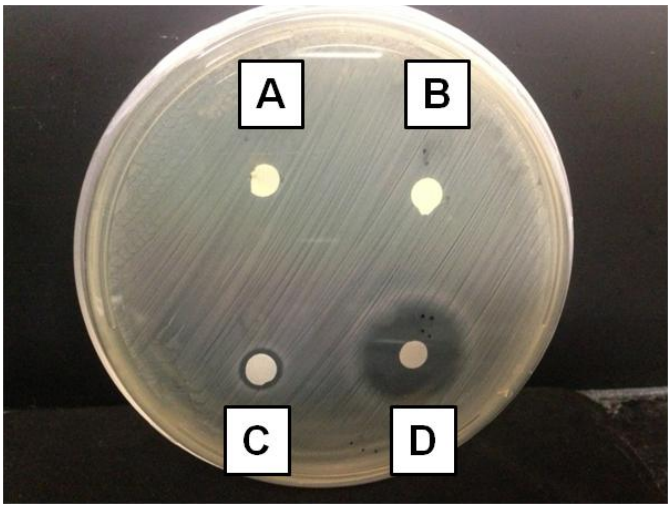

Figure 4.2: Inhibition zone of **(A)** 6% PU, **(B)** 6% PU loaded with nanoparticle, **(C)** 6%PU loaded with antibiotic drug (1% Vancomycin) and **(D)** 6%PU loaded with antibiotic drug (1% Tigecycline) on *S.Aureus* after 24 hours of incubation.

Table 4.1: Inhibition zone radius in mm of **(A)** 6% PU, **(B)** 6% PU loaded with nanoparticle, **(C)** 6%PU loaded with antibiotic drug (1% Vancomycin) and **(D)** 6%PU loaded with antibiotic drug (1% Tigecycline) with *S.Aureus* after 24 hrs incubation.

Samples	Type	Loaded with	Inhibition (mm)
A	6%PU	-	-
B		10% NPs containing Temporin A	-
C		1% Vancomycin	8.09 ± 0.41
D		1% Tigecycline	19.36 ± 0.76

As shown in Figure 4.3, PU loaded with 1% Tigecycline containing difference types of antimicrobial peptide (LL-37 and Temporin A) enhanced the inhibition zone of

S.Aureus compared to PU alone and PU loaded with 1%Tigecycline only. The reason behind this phenomenon is the MIC of each antimicrobial peptide is varied. There are many reports about the MIC of these peptides to the specific bacteria strain, in our case *(S.aureus)* it has been reported that the MIC values of LL-37 and Temporin-A are around 30 µg/ml and 50 µg/ml respectively. Therefore, the inhibition zone of *S.aureus* in PU loaded 1%Tigecycline exhibited and 20% of nanoparticle containing antimicrobial peptide LL-37 was larger than the inhibition zone of PU loaded 1%Tigecycline exhibited and 20% of nanoparticle containing antimicrobial peptide Temporin-A.

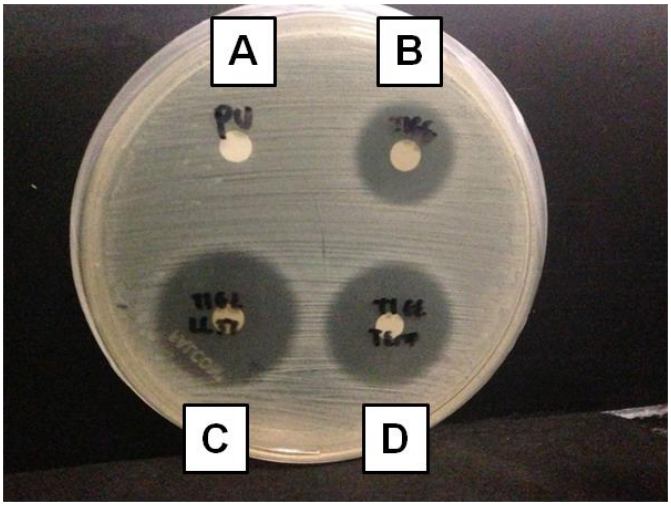

Figure 4.3: Inhibition zone of **(A)** 6% PU, **(B)** 6% PU loaded with antibiotic (1% Tigecycline), **(C)** 6%PU loaded with antibiotic drug (1% Tigecycline) and nanoparticle containing antimicrobial peptide (LL-37) and **(D)** 6%PU loaded with antibiotic drug (1% Tigecycline) and nanoparticle containing antimicrobial peptide (Temporin A) with *S.Aureus* after 24 hours of incubation.

To determine the inhibitory activity of the drug, Table 4.2 revealed the inhibition zone in term of radius (mm) of the samples. PU loaded with 1%Tigecycline and 20% of

nanoparticles containing antimicrobial peptides LL-37 showed the zone of inhibition around 26.34±1.15 mm. Moreover, PU loaded with 1%Tigecycline and 20% of nanoparticles containing antimicrobial peptides Temporin-A revealed the zone of inhibition around 24.22±0.88 mm.

Table 4.2: Inhibition zone radius in mm of **(A)** 6% PU, **(B)** 6% PU loaded with antibiotic (1% Tigecycline), **(C)** 6%PU loaded with antibiotic drug (1% Tigecycline) and nanoparticle containing antimicrobial peptide (LL-37) and **(D)** 6%PU loaded with antibiotic drug (1% Tigecycline) and nanoparticle containing antimicrobial peptide (Temporin A) with *S.Aureus* after 24 hrs incubation.

Samples	Type	Loaded with	Inhibition (mm)
A	6%PU	-	-
B		1% Tigecycline	19.36 ± 0.76
C		1% Tigecycline + 20% LL-37 NPs	26.34 ± 1.15
D		1% Tigecycline + 20% Temporin-A NPs	24.22 ± 0.88

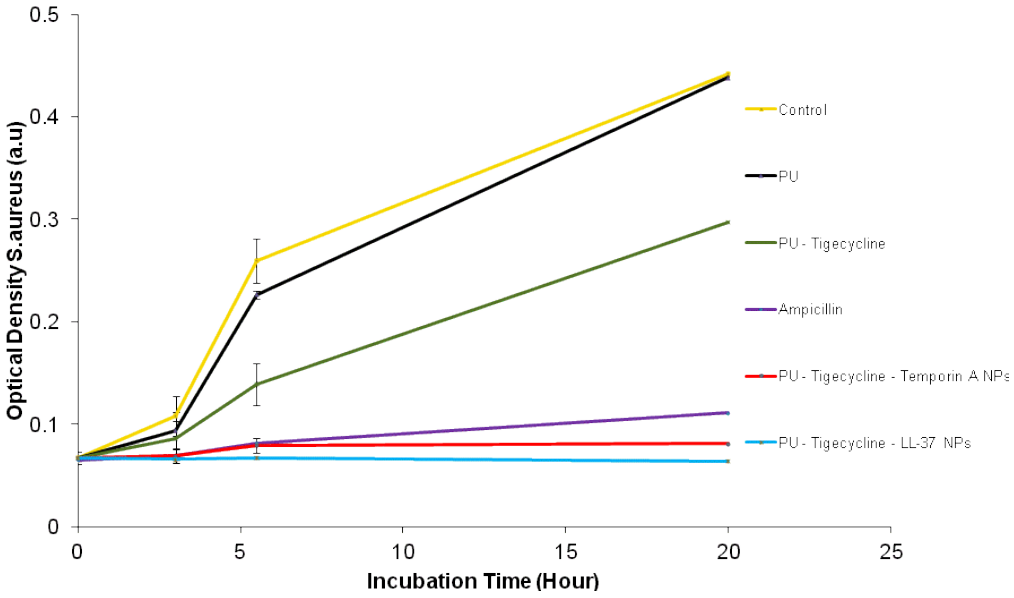

Figure 4.4: Bacteria growth curve of negative control (bacteria only), PU alone, PU loaded with Tigecycline, PU loaded with Tigecycline and nanoparticles containing Temporin-A , PU loaded with Tigecycline and nanoparticles containing LL-37, and positive control (bacteria with Ampicillin).

Bacterial growth curve was performed to assess the antibacterial activity of our scaffolds. As shown in Figure 4.4, negative control (without any treatment) and PU alone revealed the bacteria growth overtime base on the increasing trend of the absorbance value at 600 nm. With the incorporation of Tigecycline into PU nanofibrous sheet, the absorbance value was slightly decreased in the first 6h and dramatically decreased thereafter compared to those of bacteria alone or PU only indicating the less bacteria growth compared to those of control and PU alone. In the case of PU loaded with Tigecycline and nanoparticles containing Temporin-A, the absorbance value was barely increase in the first 6h and continue this trend until 20h exhibit the inhibition activity. Last but not least, the absorbance value maintain similar value from the start until 20h of

incubation in PU loaded with Tigecycline and nanoparticle containing LL-37 showing killing potential of bacteria cell in bacteria solution.

Antibiotic drug has been widely used to kill the bacteria pathogen nowadays. The severity of the pathogen and choosing type of drug are the crucial decision to make for treating patients. Each type of drugs has been revealed difference kind of effect, mechanism and killing potential. As we can observe from our results, polyurethane nanofibrous scaffolds loaded with Vancomycin demonstrated the average inhibition zone around 8.09 mm, but Tigecycline reveal the average inhibition zone around 19.36 mm. The main reason behind this phenomenon is the minimal inhibitory concentration or MIC. MIC of the various antibiotic drug has been shown difference value base on the drug mechanism and behavior. In this case, Tigecycline has been revealed the lower MIC value than Vancomycin which correlated to our results.

Antimicrobial peptide is one of options for preventing and killing bacteria pathogen. The most beneficial of antimicrobial peptide is less toxicity than antibiotic drug. However, the MIC values of antimicrobial peptides are higher than antibiotic drugs in general. We did not observe any inhibition zone for samples with nanoparticles containing antimicrobial peptides, and this could be explained by two major factors. The first factor is the concentration of the peptide which is loaded in nanoparticle was lower than MIC value. The second factor is the releasing time of the peptide. Antimicrobial peptide was loaded into nanoparticles and incorporates within nanofibrous sheets, thus there is several mechanism of releasing peptides from nanoparticles to nanofibrous sheets to the target area. To achieve the goal and overcome this obstacle, increase the amount of nanoparticles loaded into nanofibrous scaffolds might be the best option to observe the inhibition zone of bacteria pathogen.

4.3.4 Summary of preliminary results

Nanofibrous scaffolds loaded with nanoparticles containing antimicrobial peptides and/or incorporated with antibiotic drugs can be synthesized by an electrospinning technique. The scaffold fiber has been revealed the smooth morphology under SEM microscopy without beads and the diameter of the fiber were around 400-800 nm. Incorporating of antibiotic drugs into polyurethane nanofibrous scaffolds has the antibacterial property, which has been shown in the zone of inhibition of *S.Aureus* after 24 hours of incubation. Combining nanoparticle containing antimicrobial peptides into polyurethane incorporated with antibiotic drugs enhance the bacteria gram positive inhibition activity. For antimicrobial peptide loaded nanoparticles/PU fibrous sheets, it still is not ideal for anti-infection use. It requires further improvement to promote its success.

References

1. Whitesides, G. M. (2003). The'right'size in nanobiotechnology. Nature biotechnology, 21(10), 1161-1165.

2. Laval, J. M., Mazeran, P. E., & Thomas, D. (2000). Nanobiotechnology and its role in the development of new analytical devicesPresented at SAC 99, Dublin, Ireland, July 25–30, 1999. Analyst, 125(1), 29-33.

3. Zhang, L., & Webster, T. J. (2009). Nanotechnology and nanomaterials: promises for improved tissue regeneration. Nano Today, 4(1), 66-80.

4. Xu, T., Zhang, N., Nichols, H. L., Shi, D., & Wen, X. (2007). Modification of nanostructured materials for biomedical applications. Materials Science and Engineering: C, 27(3), 579-594.

5. Ramakrishna, S., Mayer, J., Wintermantel, E., & Leong, K. W. (2001). Biomedical applications of polymer-composite materials: a review. Composites science and technology, 61(9), 1189-1224.

6. Nerem, R. M. (1992). Tissue engineering in the USA. Medical and Biological Engineering and Computing, 30(4), CE8-CE12.

7. Patil, S., Li, Z., & Chan, C. (2006). Cellular to tissue informatics: approaches to optimizing cellular function of engineered tissue. In Tissue Engineering I (pp. 139-159). Springer Berlin Heidelberg.

8. Priya, S. G., Jungvid, H., & Kumar, A. (2008). Skin tissue engineering for tissue repair and regeneration. Tissue Engineering Part B: Reviews, 14(1), 105-118.

9. Vats, A., Tolley, N. S., Polak, J. M., & Gough, J. E. (2003). Scaffolds and biomaterials for tissue engineering: a review of clinical applications. Clinical Otolaryngology & Allied Sciences, 28(3), 165-172.

10. Roger VrL, Go AS, Lloyd-Jones DM, Benjamin EJ, Berry JD, Borden WB, et al. Heart Disease and Stroke Statisticsâ€”2012 Update: A Report From the American Heart Association. Circulation;125:e2-e220.

11. Koch S, Flanagan TC, Sachweh JS, Tanios F, Schnoering H, Deichmann T, et al. Fibrin-polylactide-based tissue-engineered vascular graft in the arterial circulation. Biomaterials;31:4731-9.

12. Bailey SR, Polan JL, Munoz OC, Agrawal MC, Goswami NJ. Proliferation and Î²-tubulin for human aortic endothelial cells within gas-plasma scaffolds. Cardiovascular Radiation Medicine 2004;5:119-24.

13. Gao J, Crapo P, Nerem R, Wang Y. Co-expression of elastin and collagen leads to highly compliant engineered blood vessels. Journal of Biomedical Materials Research Part A 2008;85A:1120-8.

14. Nottelet B, Pektok E, Mandracchia D, Tille JC, Walpoth B, Gurny R, et al. Factorial design optimization and in vivo feasibility of poly(ε-caprolactone)-micro- and nanofiber-based small diameter vascular grafts. Journal of Biomedical Materials Research Part A 2009;89A:865-75.

15. Hong Y, Ye S-H, Nieponice A, Soletti L, Vorp DA, Wagner WR. A small diameter, fibrous vascular conduit generated from a poly(ester urethane)urea and phospholipid polymer blend. Biomaterials 2009;30:2457-67.

16. Newby, A. C., & Zaltsman, A. B. (2000). Molecular mechanisms in intimal hyperplasia. The Journal of pathology, 190(3), 300-309.

17. Timpl, R. (1996). Macromolecular organization of basement membranes. Current opinion in cell biology, 8(5), 618-624.

18. Kraiss, L. W., & Clowes, A. W. (1997). Response of the arterial wall to injury and intimal hyperplasia. The basic science of vascular disease, 289-317.

19. Lemson, M. S., Tordoir, J. H. M., Daemen, M. J. A. P., & Kitslaar, P. J. E. H. M. (2000). Intimal hyperplasia in vascular grafts. European Journal of Vascular and Endovascular Surgery, 19(4), 336-350.

20. Schreijer, A. J., Reitsma, P. H., & Cannegieter, S. C. (2010). High hematocrit as a risk factor for venous thrombosis. Cause or innocent bystander?. Haematologica, 95(2), 182-184.

21. Wadajkar, A. S., Santimano, S., Rahimi, M., Yuan, B., Banerjee, S., & Nguyen, K. T. (2013). Deep vein thrombosis: Current status and nanotechnology advances. Biotechnology advances, 31(5), 504-513.

22. Zaucha, M. T., Gauvin, R., Auger, F. A., Germain, L., & Gleason, R. L. (2010). Biaxial biomechanical properties of self-assembly tissue-engineered blood vessels. Journal of The Royal Society Interface, rsif20100228.

23. Kannan, R. Y., Salacinski, H. J., Butler, P. E., Hamilton, G., & Seifalian, A. M. (2005). Current status of prosthetic bypass grafts: a review. Journal of Biomedical Materials Research Part B: Applied Biomaterials, 74(1), 570-581.

24. Boss, A., & Stierli, P. (1993). [Dacron prosthesis dilatation. Case report and review of the literature]. Helvetica chirurgica acta, 60(1-2), 153-156.

25. Ravi, S., & Chaikof, E. L. (2010). Biomaterials for vascular tissue engineering. Regenerative medicine, 5(1), 107-120.

26. Shinoka, T., Shum-Tim, D., Ma, P. X., Tanel, R. E., Isogai, N., Langer, R., ... & Mayer, J. E. (1998). Creation of viable pulmonary artery autografts through tissue engineering. The Journal of thoracic and cardiovascular surgery, 115(3), 536-546.

27. Watanabe, M., Shin'oka, T., Tohyama, S., Hibino, N., Konuma, T., Matsumura, G., ... & Ikada, Y. (2001). Tissue-engineered vascular autograft: inferior vena cava replacement in a dog model. Tissue engineering, 7(4), 429-439.

28. Rabe, K. F., Hurd, S., Anzueto, A., Barnes, P. J., Buist, S. A., Calverley, P., ... & Zielinski, J. (2007). Global strategy for the diagnosis, management, and prevention of chronic obstructive pulmonary disease: GOLD executive summary. American journal of respiratory and critical care medicine, 176(6), 532-555.

29. Barnes, P. J., & Stockley, R. A. (2005). COPD: current therapeutic interventions and future approaches. European Respiratory Journal, 25(6), 1084-1106.

30. Sung, J. C., Pulliam, B. L., & Edwards, D. A. (2007). Nanoparticles for drug delivery to the lungs. Trends in biotechnology, 25(12), 563-570.

31. Tahara, K., Sakai, T., Yamamoto, H., Takeuchi, H., Hirashima, N., & Kawashima, Y. (2009). Improved cellular uptake of chitosan-modified PLGA nanospheres by A549 cells. International journal of pharmaceutics, 382(1), 198-204.

32. Yamamoto, H., Kuno, Y., Sugimoto, S., Takeuchi, H., & Kawashima, Y. (2005). Surface-modified PLGA nanosphere with chitosan improved pulmonary delivery of calcitonin by mucoadhesion and opening of the intercellular tight junctions. Journal of controlled Release, 102(2), 373-381.

33. Ragab, D. M., Rohani, S., & Consta, S. (2012). Controlled release of 5-fluorouracil and progesterone from magnetic nanoaggregates. International journal of nanomedicine, 7, 3167.

34. Jones, B. G., Dickinson, P. A., Gumbleton, M., & Kellaway, I. W. (2002). Lung surfactant phospholipids inhibit the uptake of respirable microspheres by the alveolar macrophage NR8383. Journal of pharmacy and pharmacology, 54(8), 1065-1072.

35. Jones, B. G., Dickinson, P. A., Gumbleton, M., & Kellaway, I. W. (2002). The inhibition of phagocytosis of respirable microspheres by alveolar and peritoneal macrophages. International journal of pharmaceutics, 236(1), 65-79.

36. El-Sherbiny, I. M., El-Baz, N. M., & Yacoub, M. H. (2015). Inhaled nano-and microparticles for drug delivery. Global cardiology science & practice, 2015.

37. Akbarzadeh, A., Rezaei-Sadabady, R., Davaran, S., Joo, S. W., Zarghami, N., Hanifehpour, Y., ... & Nejati-Koshki, K. (2013). Liposome: classification, preparation, and applications. Nanoscale research letters, 8(1), 1.

38. Yokoyama, M. (2011). Clinical applications of polymeric micelle carrier systems in chemotherapy and image diagnosis of solid tumors. Journal of Experimental & Clinical Medicine, 3(4), 151-158.

39. Chakravarthi, S. S., Robinson, D. H., & De, S. (2007). Nanoparticles prepared using natural and synthetic polymers. Drugs and the pharmaceutical sciences, 166, 51.

40. Centers for Disease Control and Prevention (CDC). (2012). National diabetes fact sheet: national estimates and general information on diabetes and prediabetes in the United States, 2011. Atlanta, GA: US Department of Health and Human Services, Centers for Disease Control and Prevention; 2011.

41. Boateng, J. S., Matthews, K. H., Stevens, H. N., & Eccleston, G. M. (2008). Wound healing dressings and drug delivery systems: a review. Journal of pharmaceutical sciences, 97(8), 2892-2923.

42. Schultz, G. S. (1999). Molecular regulation of wound healing. Acute and chronic wounds: Nursing management. 2nd edition. St. Louis, MO: Mosby, 413-429.

43. Halim, A. S., Khoo, T. L., & Shah, J. M. Y. (2010). Biologic and synthetic skin substitutes: an overview. Indian Journal of Plastic Surgery, 43(3), 23.

44. Madaghiele, M., Demitri, C., Sannino, A., & Ambrosio, L. (2015). Polymeric hydrogels for burn wound care: Advanced skin wound dressings and regenerative templates. Burns & Trauma, 2(4), 153.

45. McCarty, S. M., & Percival, S. L. (2013). Proteases and delayed wound healing. Advances in wound care, 2(8), 438-447.

46. Roger, V. L., Go, A. S., Lloyd-Jones, D. M., Benjamin, E. J., Berry, J. D., Borden, W. B., ... & Turner, M. B. (2012). Heart disease and stroke statistics—2012 update a report from the American heart association. Circulation, 125(1), e2-e220.

47. Wang, X., Lin, P., Yao, Q., & Chen, C. (2007). Development of small-diameter vascular grafts. World journal of surgery, 31(4), 682-689.

48. Koch, S., Flanagan, T. C., Sachweh, J. S., Tanios, F., Schnoering, H., Deichmann, T., ... & Jockenhoevel, S. (2010). Fibrin-polylactide-based tissue-engineered vascular graft in the arterial circulation. Biomaterials, 31(17), 4731-4739.

49. Bailey, S. R., Polan, J. L., Munoz, O. C., Agrawal, M. C., & Goswami, N. J. (2004). Proliferation and β-tubulin for human aortic endothelial cells within gas-plasma scaffolds. Cardiovascular radiation medicine, 5(3), 119-124.

50. Gao, J., Crapo, P., Nerem, R., & Wang, Y. (2008). Co-expression of elastin and collagen leads to highly compliant engineered blood vessels. Journal of biomedical materials research Part A, 85(4), 1120-1128.

51. Nottelet, B., Pektok, E., Mandracchia, D., Tille, J. C., Walpoth, B., Gurny, R., & Moeller, M. (2009). Factorial design optimization and in vivo feasibility of poly (ε-caprolactone)-micro-and nanofiber-based small diameter vascular grafts. Journal of Biomedical Materials Research Part A, 89(4), 865-875.

52. Mrówczyński, W., Mugnai, D., de Valence, S., Tille, J. C., Khabiri, E., Cikirikcioglu, M., ... & Walpoth, B. H. (2014). Porcine carotid artery replacement with

biodegradable electrospun poly-e-caprolactone vascular prosthesis. Journal of vascular surgery, 59(1), 210-219.

53. Hong, Y., Ye, S. H., Nieponice, A., Soletti, L., Vorp, D. A., & Wagner, W. R. (2009). A small diameter, fibrous vascular conduit generated from a poly (ester urethane) urea and phospholipid polymer blend. Biomaterials, 30(13), 2457-2467.

54. Soletti, L., Nieponice, A., Hong, Y., Ye, S. H., Stankus, J. J., Wagner, W. R., & Vorp, D. A. (2011). In vivo performance of a phospholipid-coated bioerodable elastomeric graft for small-diameter vascular applications. Journal of Biomedical Materials Research Part A, 96(2), 436-448.

55. Wu, W., Allen, R. A., & Wang, Y. (2012). Fast-degrading elastomer enables rapid remodeling of a cell-free synthetic graft into a neoartery. Nature medicine, 18(7), 1148-1153.

56. Blit, P. H., McClung, W. G., Brash, J. L., Woodhouse, K. A., & Santerre, J. P. (2011). Platelet inhibition and endothelial cell adhesion on elastin-like polypeptide surface modified materials. Biomaterials, 32(25), 5790-5800.

57. Hong, Y., Ye, S. H., Pelinescu, A. L., & Wagner, W. R. (2012). Synthesis, characterization, and paclitaxel release from a biodegradable, elastomeric, poly (ester urethane) urea bearing phosphorylcholine groups for reduced thrombogenicity. Biomacromolecules, 13(11), 3686-3694.

58. Jun, H. W., Taite, L. J., & West, J. L. (2005). Nitric oxide-producing polyurethanes. Biomacromolecules, 6(2), 838-844.

59. Lipke, E. A., & West, J. L. (2005). Localized delivery of nitric oxide from hydrogels inhibits neointima formation in a rat carotid balloon injury model. Acta biomaterialia, 1(6), 597-606.

60. Taite, L. J., Yang, P., Jun, H. W., & West, J. L. (2008). Nitric oxide-releasing polyurethane–PEG copolymer containing the YIGSR peptide promotes endothelialization with decreased platelet adhesion. Journal of Biomedical Materials Research Part B: Applied Biomaterials, 84(1), 108-116.

61. Luong-Van, E., Grøndahl, L., Chua, K. N., Leong, K. W., Nurcombe, V., & Cool, S. M. (2006). Controlled release of heparin from poly (ε-caprolactone) electrospun fibers. Biomaterials, 27(9), 2042-2050.

62. Del Gaudio, C., Ercolani, E., Galloni, P., Santilli, F., Baiguera, S., Polizzi, L., & Bianco, A. (2013). Aspirin-loaded electrospun poly (ε-caprolactone) tubular scaffolds: potential small-diameter vascular grafts for thrombosis prevention.*Journal of Materials Science: Materials in Medicine*, *24*(2), 523-532.

63. Innocente, F., Mandracchia, D., Pektok, E., Nottelet, B., Tille, J. C., De Valence, S., ... & Walpoth, B. H. (2009). Paclitaxel-Eluting biodegradable synthetic vascular prostheses a step towards reduction of neointima formation?. Circulation, 120(11 suppl 1), S37-S45.

64. Aldenhoff, Y. B., van der Veen, F. H., ter Woorst, J., Habets, J., Poole–Warren, L. A., & Koole, L. H. (2001). Performance of a polyurethane vascular prosthesis carrying a dipyridamole (Persantin®) coating on its lumenal surface. Journal of biomedical materials research, 54(2), 224-233.

65. Muller, T. H., Su, C. A., Weisenberger, H., Brickl, R., Nehmiz, G., & Eisert, W. G. (1990). Dipyridamole alone or combined with low-dose acetylsalicylic acid inhibits platelet aggregation in human whole blood ex vivo [see comments]. British journal of clinical pharmacology, 30(2), 179-186.

66. Singh, J. P., Rothfuss, K. J., Wiernicki, T. R., Lacefield, W. B., Kurtz, L., Brown, R. F., ... & Dubé, G. P. (1994). Dipyridamole directly inhibits vascular smooth muscle

cell proliferation in vitro and in vivo: implications in the treatment of restenosis after angioplasty. Journal of the American College of Cardiology, 23(3), 665-671.

67. Mattfeldt, T., Mall, G. (1983). Dipyridamole-induced capillary endothelial cell proliferation in the rat heart—a morphometric investigation. Cardiovascular research, 17(4), 229-237.

68. Zhuplatov, S. B., Masaki, T., Blumenthal, D. K., & Cheung, A. K. (2006). Mechanism of dipyridamole's action in inhibition of venous and arterial smooth muscle cell proliferation. Basic & clinical pharmacology & toxicology, 99(6), 431-439.

69. Guan, J., Sacks, M. S., Beckman, E. J., & Wagner, W. R. (2002). Synthesis, characterization, and cytocompatibility of elastomeric, biodegradable poly (ester-urethane) ureas based on poly (caprolactone) and putrescine. Journal of biomedical materials research, 61(3), 493-503.

70. Hong, Y., Huber, A., Takanari, K., Amoroso, N. J., Hashizume, R., Badylak, S. F., & Wagner, W. R. (2011). Mechanical properties and in vivo behavior of a biodegradable synthetic polymer microfiber–extracellular matrix hydrogel biohybrid scaffold. Biomaterials, 32(13), 3387-3394.

71. Zhu, G., Ju, H., & Zheng, H. (2004). Fluorescence spectroscopic determination of dipyridamole binding on pancreas-1 tumor cell membrane. Clinica chimica acta, 348(1), 101-106.

72. Dey, J., Xu, H., Nguyen, K. T., & Yang, J. (2010). Crosslinked urethane doped polyester biphasic scaffolds: potential for in vivo vascular tissue engineering. Journal of Biomedical Materials Research Part A, 95(2), 361-370.

73. Motlagh, D., Yang, J., Lui, K. Y., Webb, A. R., & Ameer, G. A. (2006). Hemocompatibility evaluation of poly (glycerol-sebacate) in vitro for vascular tissue engineering. Biomaterials, 27(24), 4315-4324.

74. Nie, S., Xue, J., Lu, Y., Liu, Y., Wang, D., Sun, S., ... & Zhao, C. (2012). Improved blood compatibility of polyethersulfone membrane with a hydrophilic and anionic surface. Colloids and Surfaces B: Biointerfaces, 100, 116-125.

75. Dey, J., Xu, H., Shen, J., Thevenot, P., Gondi, S. R., Nguyen, K. T., ... & Yang, J. (2008). Development of biodegradable crosslinked urethane-doped polyester elastomers. Biomaterials, 29(35), 4637-4649.

76. Tsushima, K., King, L. S., Aggarwal, N. R., De Gorordo, A., D'Alessio, F. R., & Kubo, K. (2009). Acute lung injury review. Internal Medicine, 48(9), 621-630.

77. Azarmi, S., Roa, W. H., & Löbenberg, R. (2008). Targeted delivery of nanoparticles for the treatment of lung diseases. Advanced drug delivery reviews, 60(8), 863-875.

78. Zahoor, A., Sharma, S., & Khuller, G. K. (2005). Inhalable alginate nanoparticles as antitubercular drug carriers against experimental tuberculosis. International journal of antimicrobial agents, 26(4), 298-303.

79. Pandey, R., Sharma, A., Zahoor, A., Sharma, S., Khuller, G. K., & Prasad, B. (2003). Poly (DL-lactide-co-glycolide) nanoparticle-based inhalable sustained drug delivery system for experimental tuberculosis. Journal of Antimicrobial Chemotherapy, 52(6), 981-986.

80. Sharma, A., Sharma, S., & Khuller, G. K. (2004). Lectin-functionalized poly (lactide-co-glycolide) nanoparticles as oral/aerosolized antitubercular drug carriers for treatment of tuberculosis. Journal of antimicrobial chemotherapy, 54(4), 761-766.

81. Jones, B. G., Dickinson, P. A., Gumbleton, M., & Kellaway, I. W. (2002). Lung surfactant phospholipids inhibit the uptake of respirable microspheres by the alveolar macrophage NR8383. Journal of pharmacy and pharmacology, 54(8), 1065-1072.

82. Hoshiba, T., Lu, H., Kawazoe, N., & Chen, G. (2010). Decellularized matrices for tissue engineering. Expert opinion on biological therapy, 10(12), 1717-1728.

83. Badylak, S. F., Freytes, D. O., & Gilbert, T. W. (2009). Extracellular matrix as a biological scaffold material: structure and function. Acta biomaterialia, 5(1), 1-13.

84. Bader, A., Schilling, T., Teebken, O. E., Brandes, G., Herden, T., Steinhoff, G., & Haverich, A. (1998). Tissue engineering of heart valves–human endothelial cell seeding of detergent acellularized porcine valves. European journal of cardio-thoracic surgery, 14(3), 279-284.

85. Syedain, Z. H., Bradee, A. R., Kren, S., Taylor, D. A., & Tranquillo, R. T. (2012). Decellularized tissue-engineered heart valve leaflets with recellularization potential. Tissue Engineering Part A, 19(5-6), 759-769.

86. Booth, C., Korossis, S. A., Wilcox, H. E., Watterson, K. G., Kearney, J. N., Fisher, J., & Ingham, E. (2002). Tissue engineering of cardiac valve prostheses I: development and histological characterization of an acellular porcine scaffold. The Journal of heart valve disease, 11(4), 457-462.

87. Lin, P., Chan, W. C., Badylak, S. F., & Bhatia, S. N. (2004). Assessing porcine liver-derived biomatrix for hepatic tissue engineering. Tissue engineering, 10(7-8), 1046-1053.

88. Liu, Y., Bharadwaj, S., Lee, S. J., Atala, A., & Zhang, Y. (2009). Optimization of a natural collagen scaffold to aid cell–matrix penetration for urologic tissue engineering. Biomaterials, 30(23), 3865-3873.

89. Benders, K. E., van Weeren, P. R., Badylak, S. F., Saris, D. B., Dhert, W. J., & Malda, J. (2013). Extracellular matrix scaffolds for cartilage and bone regeneration. Trends in biotechnology, 31(3), 169-176.

90. Brown, B. N., & Badylak, S. F. (2014). Extracellular matrix as an inductive scaffold for functional tissue reconstruction. Translational Research, 163(4), 268-285.

91. Faulk, D. M., Johnson, S. A., Zhang, L., & Badylak, S. F. (2014). Role of the extracellular matrix in whole organ engineering. Journal of cellular physiology, 229(8), 984-989.

92. Volpato, F. Z., Führmann, T., Migliaresi, C., Hutmacher, D. W., & Dalton, P. D. (2013). Using extracellular matrix for regenerative medicine in the spinal cord. Biomaterials, 34(21), 4945-4955.

93. Ingenito, E. P., Sen, E., Tsai, L. W., Murthy, S., & Hoffman, A. (2010). Design and testing of biological scaffolds for delivering reparative cells to target sites in the lung. Journal of tissue engineering and regenerative medicine, 4(4), 259-272.

94. Lin, Y. M., Zhang, A., Rippon, H. J., Bismarck, A., & Bishop, A. E. (2010). Tissue engineering of lung: the effect of extracellular matrix on the differentiation of embryonic stem cells to pneumocytes. Tissue Engineering Part A, 16(5), 1515-1526.

95. Kelleher, C. M., & Vacanti, J. P. (2010). Engineering extracellular matrix through nanotechnology. Journal of The Royal Society Interface, rsif20100345.

96. Wu, J., Ding, Q., Dutta, A., Wang, Y., Huang, Y. H., Weng, H., ... & Hong, Y. (2015). An injectable extracellular matrix derived hydrogel for meniscus repair and regeneration. Acta biomaterialia, 16, 49-59.

97. Menon, J. U., Kona, S., Wadajkar, A. S., Desai, F., Vadla, A., & Nguyen, K. T. (2012). Effects of surfactants on the properties of PLGA nanoparticles. Journal of biomedical materials research Part A, 100(8), 1998-2005.

98. Menon, J. U., Ravikumar, P., Pise, A., Gyawali, D., Hsia, C. C., & Nguyen, K. T. (2014). Polymeric nanoparticles for pulmonary protein and DNA delivery. Acta biomaterialia, 10(6), 2643-2652.

99. Zhou, Y. M., Shan, Y., Sun, Y. Q., & Ju, H. X. (2008). Adsorption of collagen to indium oxide nanoparticles and infrared emissivity study thereon. Materials Research Bulletin, 43(8), 2105-2112.

100. Martin, P. (1997). Wound healing--aiming for perfect skin regeneration. Science, 276(5309), 75-81.

101. Ovington, L. G. (2007). Advances in wound dressings. Clinics in dermatology, 25(1), 33-38.

102. Hollander, D. A., Soranzo, C., Falk, S., & Windolf, J. (2001). Extensive traumatic soft tissue loss: reconstruction in severely injured patients using cultured hyaluronan-based three-dimensional dermal and epidermal autografts. Journal of Trauma and Acute Care Surgery, 50(6), 1125-1136.

103. Doillon, C. J., Whyne, C. F., Brandwein, S., & Silver, F. H. (1986). Collagen-based wound dressings: Control of the pore structure and morphology. Journal of biomedical materials research, 20(8), 1219-1228.

104. Murakami, K., Aoki, H., Nakamura, S., Nakamura, S. I., Takikawa, M., Hanzawa, M., ... & Ishihara, M. (2010). Hydrogel blends of chitin/chitosan, fucoidan and alginate as healing-impaired wound dressings. Biomaterials, 31(1), 83-90.

105. Zhong, S. P., Zhang, Y. Z., & Lim, C. T. (2010). Tissue scaffolds for skin wound healing and dermal reconstruction. Wiley Interdisciplinary Reviews: Nanomedicine and Nanobiotechnology, 2(5), 510-525.

106. Chua, A. W. C., Ma, D. R., Song, I. C., Phan, T. T., Lee, S. T., & Song, C. (2008). In vitro evaluation of fibrin mat and Tegaderm™ wound dressing for the delivery of keratinocytes—Implications of their use to treat burns. Burns, 34(2), 175-180.

107. Chen, G., Sato, T., Ohgushi, H., Ushida, T., Tateishi, T., & Tanaka, J. (2005). Culturing of skin fibroblasts in a thin PLGA–collagen hybrid mesh. *Biomaterials*,*26*(15), 2559-2566.

108. Dai, N. T., Williamson, M. R., Khammo, N., Adams, E. F., & Coombes, A. G. A. (2004). Composite cell support membranes based on collagen and polycaprolactone for tissue engineering of skin. Biomaterials, 25(18), 4263-4271.

109. Said, S. S., El-Halfawy, O. M., El-Gowelli, H. M., Aloufy, A. K., Boraei, N. A., & El-Khordagui, L. K. (2012). Bioburden-responsive antimicrobial PLGA ultrafine fibers for wound healing. European Journal of Pharmaceutics and Biopharmaceutics, 80(1), 85-94.

110. Choi, J. S., Leong, K. W., & Yoo, H. S. (2008). In vivo wound healing of diabetic ulcers using electrospun nanofibers immobilized with human epidermal growth factor (EGF). Biomaterials, 29(5), 587-596.

111. Song, A., Rane, A. A., & Christman, K. L. (2012). Antibacterial and cell-adhesive polypeptide and poly (ethylene glycol) hydrogel as a potential scaffold for wound healing. Acta biomaterialia, 8(1), 41-50.

Biographical Information

Primana Punnakitikashem was born in 1987 in Bangkok, Thailand. He completed his B.Sc. degree in Biochemistry from Chulalongkorn University and M.S. in Logistic from University of Texas at Arlington. After his graduation, he initially worked as a volunteer in Dr.Kytai Nguyen's laboratory in the topic of nanofibrous mesh for wound healing application. Then, he started his Ph.D. career under supervising of Dr. Yi Hong and Dr. Kytai T. Nguyen. During his study, he worked on several projects as a research assistance. He developed nanostructured biomaterials for tissue regeneration and repair. He has received a few awards such as President's Poster and Provost's Poster Award from The Annual Celebration of Excellence by students' symposium at the University of Texas at Arlington.